

Superficial white matter: A review on the dMRI analysis methods and applications



Miguel Guevara^{a,*}, Pamela Guevara^b, Claudio Román^b, Jean-François Mangin^a

^a UNATI, Neurospin, CEA, Université Paris-Saclay, Gif-sur-Yvette, France

^b Faculty of Engineering, Universidad de Concepción, Concepción, Chile

ARTICLE INFO

Keywords:

Superficial white matter
Diffusion-weighted imaging
Tractography
White matter bundle
U-fibers
Short association fibers

ABSTRACT

The mapping of human brain connections is still an on going task. Unlike deep white matter (DWM), which has been extensively studied and well documented, superficial white matter (SWM) has been often left aside. Improving our understanding of the SWM is an important goal for a better understanding of the brain network and its relation to several pathologies. The shape and localization of these short bundles present a high variability across subjects. Furthermore, the small diameter of most superficial bundles and partial volume effects induced by their proximity to the cortex leads to complex tractography issues. Therefore, the mapping of SWM bundles and the use of the resulting atlases for clinical studies require dedicated methodologies that are reviewed in this paper.

1. Introduction

The cartography of the macroscopic connection of the human brain is still incomplete. Mapping this network called human brain structural connectome is essential for a better understanding of the brain function and pathologies (Sporns et al., 2005). In the past, white matter (WM) has been mainly studied by means of postmortem dissections, in order to document the main pathways. This kind of studies allowed a rough classification of the WM into projection, commissural and association connections. The last ones are the pathways connecting different areas within a same brain hemisphere, and are often subdivided into long and short connections. Long fibers connect distant areas of the same hemisphere by leaving the cortex and traversing the depth of the hemisphere white matter, reason why they are also known as deep white matter (DWM). They organize into large well-defined bundles that are stable across subjects. These features have facilitated their study, by means of postmortem dissections and diffusion MRI (dMRI), and therefore their description is well documented. On the other hand, short connections hook-up close-by areas (often neighboring gyri) surrounding the cortex sulci, and they are also known as superficial white matter (SWM) or U-fibers. Unlike DWM, little is known about SWM fasciculi since their small size and their proximity to the cortex pose a challenge to their study. In terms of postmortem studies, those features make difficult their dissection by removing the cortex without interfering with the fibers configuration. These structures are among the last parts of the brain to

myelinate, process which may extend into the fourth decade of life, making these bundles more vulnerable to damage during the brain maturation (Wu et al., 2014). Although their general function is still unknown, their relationship with different pathologies has been described in some studies. For instance an overconnectivity of some SWM bundles was found in autism spectrum disorder (Zikopoulos and Barbas, 2013). Other studies have described a lower connectivity in the frontal region for diseases as schizophrenia, attention deficit disorder, dyslexia, down syndrome, depression and HIV/AIDS (Fröhlich, 2016).

One of the first anatomists that mentioned the existence of the SWM was Henry Gray in 1858 (Gray, 1878). He vaguely described short association fibers as those placed immediately underneath the gray matter of the cortex and that they connect adjacent gyri. Later on, in 1885 Theodor Meynert described archiform fibers or *fibræ propiæ* of the cortex, as those right next to the cortical substance, separating it from its adjoining white matter (Meynert, 1885). He reports that these fiber bundles have different sizes, as they do not only connect adjacent gyri but also can skip one, two or more series of convolutions. The shortest ones are the nearest to the cortex and present the characteristic U-shape, due to their closeness to the walls of the convolution depression. The emergence of dMRI in the early 1990s enabled the study of WM tracts, and in particular, SWM in vivo. One of the first works that analyzed SWM appearance in diffusion images was the study performed by Pierpaoli et al., in 1996 (Pierpaoli et al., 1996), describing them as structures with high hyperintensity due to the highly ordered fiber tracts. Next, in 1999,

* Corresponding author.

E-mail address: mguevara.bme@gmail.com (M. Guevara).

Conturo et al. proposed one of the earliest works using tractography to identify WM bundles, including some U-fibers (Conturo et al., 1999). They exposed the feasibility of tracking these complex structures, where the anisotropy is lower than in DWM. One of the first studies describing SWM bundles was carried out by Catani et al., in 2003 (Catani et al., 2003), that identified a chain of U-shaped fibers running laterally to the inferior longitudinal fasciculus, that connect adjacent gyri of the lateral occipito-temporal region. For years, few studies of SWM were conducted since dMRI techniques did not allow a good reconstruction of superficial fibers, due to low acquisition quality and poor methodology to deal with fiber crossing. Nowadays, for both postmortem or dMRI-based virtual dissections new techniques are available, that allow a better description of these complex short fasciculi.

Diffusion-weighted imaging (dMRI) allows the study of brain white matter in vivo and in a noninvasive way, by measuring the perturbations of water diffusion induced by the cellular microstructures and their anisotropies (Basser, 1995; Le Bihan et al., 2001). Therefore dMRI is the preferred method to perform white matter studies. Furthermore, this technique is a very valuable tool for the study of neuropathologies. Many of the brain diseases and disorders present changes in water diffusion, which can be simply established through dMRI-based indices. The water diffusion anisotropy can lead to fiber orientation models used to perform fiber tractography, namely step by step reconstruction of the putative 3D trajectory of the fiber bundles (Mori and Van Zijl, 2002). These models range from the simplest historical one, that allows only the representation of the main diffusion direction in each voxel (Le Bihan et al., 2001), to highly sophisticated ones allowing a better representation of complex geometries like fiber crossing or kissing (Johansen-Berg and Behrens, 2013). Using these modern local diffusion models, tractography can target not only large bundles but also the trajectories of small fasciculi, also called fibers for the sake of simplicity.

Because of numerous ambiguities, using the water diffusion signal as a proxy to fiber orientation is not prone to error, which leads to spurious trajectories at the stage of tractography. To overcome this difficulty, a wide variety of tractography algorithms have been designed, each yielding different results, which can impact qualitatively the reconstructed representations of the white matter geometry (Chung et al., 2011). The two main classes of algorithms are deterministic and probabilistic methods. Deterministic approaches follow the most likely fiber path given by the main local maxima of the fiber orientation model to reconstruct the fiber trajectories. On the other hand, for probabilistic tractography algorithms, besides this orientation estimation, there is also an estimation of the distribution of the directions around the maxima (i.e. how likely each other orientation is to lie along a fiber). Then, the connections are traced several times, each time using slightly different orientations. The set of all these different pathways are called a measure of the connection likelihood or probability (HCP). Hence probabilistic approaches yield a much greater amount of trajectories, increasing both the chances to catch all the actual bundles and the risk to detect spurious ones.

White matter fibers can be grouped into bundles of similar fibers (i.e. fibers with similar shape, size and position) connecting the same anatomical and/or functional areas. The identification of fiber bundles from tractograms, namely the whole set of trajectories resulting from tractography, is not an easy task because of the high risk of false positive. Anatomical knowledge is needed in order to identify actual anatomical structures. Many research groups have focused on developing methods to extract those bundles, either by manual identification, or using semi-automatic or automatic approaches. Whatever the tractography algorithm, the tractogram contains a large amount of spurious fibers that need to be filtered out. However, most of the existing methods developed to identify WM bundles have been designed for large DWM bundles stable across subjects. Therefore, they do not transfer well to the complex SWM fasciculi, which partly explain the low interest in their study for many years.

Nowadays, new equipment (tools) and software have been introduced

into the field of diffusion imaging. Refined acquisition methods, diffusion models and tractography algorithms have been developed, yielding improved tractograms. For instance, high angular resolution diffusion imaging (HARDI) has overcome to some extent the challenge raised by fiber crossing geometries, while keeping the acquisition time reasonable (Descoteaux et al., 2009). Therefore, during the last years, several studies have focused successfully on the study of SWM fasciculi, including applications to clinical research. Furthermore, the relationship between DWM and SWM has taken special relevance lately, as some studies have demonstrated that in many brain pathologies or disorders, the changes might not only occur in DWM but also in specific regions of the SWM. Furthermore, some developmental disorders are supposed to stem from a wrong balance between short and long connections.

In this paper we present a review of the main advances in the study of SWM using dMRI. We summarize the main methods utilized and how they relate SWM structures with clinical studies.

2. Superficial white matter analysis methods

The improvements in the last decade of dMRI acquisition and the whole processing pipeline lead to a better reconstruction of fibers, in particular short association fibers. These fibers have been studied using tools mostly developed for DWM analysis. For example a group of methods allow the grouping of fibers into anatomically meaningful fiber bundles, given specific criteria (Catani et al., 2002; Wakana et al., 2004; Wassermann et al., 2010; Zhang et al., 2008; Guevara et al., 2012; O'Donnell et al., 2006). As the anatomy of DWM bundles is well-known, algorithms lead to similar results, which has been shown in comparative studies (Zhang et al., 2019). However, the consistency across approaches raise more concerns in the case for SWM bundles. Different studies have different definitions of short association fibers (fiber length restrictions, closeness of the regions they connect, closeness to the brain cortex, etc), therefore comparisons are difficult. Depending on the type of analysis used for identifying the bundles, these methods can be divided into: (i) placement of regions of interest (ROI), which allow the extraction of fibers that fulfill a given condition; (ii) clustering of fibers, that group fibers given a fiber similarity measure; and (iii) hybrid methods which combine both of the previously mentioned approaches.

2.1. ROI placement methods

The ROI placement methods define brain areas to be used as guides for identifying specific bundles or to isolate fibers connecting a pair of specific regions. This approach provides anatomical information to the analysis, since the ROIs often define known anatomical structures or functional areas. The ROIs are used as a guide to select fibers that satisfy a given condition i.e. if fibers end in a ROI, pass through a ROI, or do not pass through a ROI (O'Donnell et al., 2013). The conditions can be combined using logical operations. For the definition of the areas, *manual*, *automatic* or a mix of both strategies have been used.

2.1.1. Manual placement

Manual ROI placement consists in meticulous delineation of anatomical regions (in a subject or group of subjects), which are often small enough to isolate a specific group of fibers, yielding precisely defined bundles. This kind of approach is highly time consuming, limiting its application to only a few subjects and a reduced amount of regions. Also, this approach depends on the expertise of the operator, which limits its reproducibility. One of the first works of this kind was the one developed by Catani et al. (2003). The fiber segmentation was performed from a DTI dataset averaged across 11 subjects, and only for the occipital and temporal regions. This work was not specifically focused on the short fibers and therefore no detailed description about them was given, just the mention of their existence within the data and a rough description of their position. In the same spirit, the work of (Wakana et al., 2004) also studied long and short fibers but in the whole brain,

from DTI data of 4 subjects. In this work the authors mention the existence of short fibers in the frontal region which might be part of the frontal superior longitudinal fasciculus, and in the occipital region. Some years later, and following the idea of their first work (Catani et al., 2003), in (Catani et al., 2012) the authors performed this time a study focused in short fibers. They performed a detailed segmentation and analysis of the short connections of the frontal and parietal lobe for a single subject with high quality HARDI data. The method was also applied to 12 subjects for lateralization analysis. This was the first study of this kind only focused on short association fibers with a strong anatomical emphasis. The bundles obtained were well characterized in terms of the specific regions they connect and the course they follow. Although this study was limited only to a specific region of the brain, the precise delineation of small ROIs allowed the authors to obtain very well-defined bundles. Also, the study of the relation of the ROIs with known functional areas provided some insights on their role in brain function. In addition, the authors performed a postmortem dissection of the tracts, providing a good validation. The bundles described in this work were later replicated in (Rojkova et al., 2016) in order to build a statistical atlas from HARDI data of 47 subjects and study their variability in terms of age and education. The creation of an atlas provides a mean to perform the segmentation of the bundles composing it in new subjects, enabling clinical (or functional) connectivity studies.

Another example of manual segmentation of short fibers is the work by Wu et al. (2016). The authors utilized regions of avoidance (ROA) (*i.e.* region used to exclude fibers passing through it) drawn in DSI studio software¹ in order to extract SWM connections. They focused in the temporal, parietal and occipital lobes. The segmentation was performed over the DSI data of 10 subjects and a publicly available template composed by 90 subjects (NTU-90 Atlas, composed by the averaged DSI data from 45 males and 45 female subjects) (Yeh and Tseng, 2011). These results were compared with previous DTI reports, evidencing that higher resolution images allow a better description of the connectivity patterns. Postmortem dissections were also performed showing high agreement with the tractography results.

Another example is exposed in (Burks et al., 2017), where the authors used 10 subjects from the HCP database to study the connections in the inferior parietal lobe. They applied user-defined seed ROIs, based on expert knowledge, in DSI studio software for tracking the fibers and isolate the tracts. These fiber tracking were also validated by postmortem dissection. The fact that this study was only focused in a specific region of the brain, allowed a good anatomical and functional description of the fiber bundles connecting the analyzed areas. The authors found short fibers connecting the supramarginal and angular gyri, and connecting both of these gyri to the superior parietal lobule. Finally, in a region-specific study of the parietal lobe (Catani et al., 2017), the authors studied short connections in human and monkey brain. This is one of the few works that compare short fiber bundles across different species. They performed the analysis over the data of 21 alive humans and 11 *ex vivo* datasets, 5 vervet and 6 macaque monkeys. As in most of manual segmentations, only few regions were considered in the study: postcentral gyrus, superior parietal lobule and inferior parietal lobule. The results show a close correspondence between the connections in human brains and in monkey brains (these connections in monkey brains have also been described by axonal tracing methods), showing the evolutionary link between these species and their implication in human functions. The authors also performed a postmortem dissection in order to keep only the bundles found both in tractography and in the actual brain. The postmortem dissection was performed based on the Klingler method (Ludwig and Karger, 1957), using the brain of a male donor. Thanks to the water crystallization process, the brain cortex can be easily removed, exposing the underlying white matter. Fiber bundles were then dissected by peeling off the white matter.

2.1.2. Automatic placement

Automatic ROI placement usually relies on templates containing the ROIs already defined, generally brain parcellations which are then automatically warped to the subject image. This kind of ROI delineation, in contrast to the manual one, can be easily extended to the whole brain and to a larger amount of subjects. One of the first SWM studies conducted using this kind of approach is described in (Oishi et al., 2008). The authors created a ROI atlas of gray and white matter, constructed from the average of 81 subjects. Then, they applied this atlas to segment the fibers from the DTI data of 10 subjects. Using their white matter parcellation as ROIs, they isolated the fibers traversing them. Although the whole brain was analyzed, only a few bundles were successfully segmented, mainly because of the type of data utilized. As mentioned before, due to SWM configuration their tractography streamlines are difficult to successfully reconstruct, especially using DTI data which does not provide enough information about the different directions present in a voxel. Also, the size of the ROIs employed only allowed a rough delineation of the bundles. The authors later expanded their work by creating a single-subject WM atlas containing 46 SWM structures (based on the previous averaged atlas) (Oishi et al., 2009). The difference with the previous work is that this time no fibers were segmented, only the voxels contained in the desired areas. The advantage of a single-subject atlas is that it contains sharper definitions of the delineated structures, unlike averaged atlas where these structures are blurred. This sharpness is specially useful for the delineation of the SWM, as it is highly variable. However, the downside of these kind of atlas is that they might contain subject-specific structures, which are not common to the rest of the population. Following this idea, another SWM study was performed for the whole brain (Zhang et al., 2010). It was conducted by first warping the same ROI atlas of (Oishi et al., 2008) into the DTI data of 20 subjects by non-linear registration. The authors looked for all possible connections between different pairs of cortical regions. These segmentations were then labeled based on the pair of ROIs they connected. The automated placement of ROIs and fibers segmentation allowed this work to be the first describing a large amount of fiber bundles. However, as in previous works, no detailed description of the bundles was given and only a rough delineation of them was presented as average density maps, due to the size of the ROIs. The existence of the connections was reported for a minimum of one fiber per connection.

Another whole brain study was the one performed in (Ouyang et al., 2016) in order to analyze the maturation index of the developmental brain. The authors segmented the brain cortex into 34 gyri per hemisphere using FreeSurfer² and the Desikan-Killiany atlas (Desikan et al., 2006) (see Table A.7) for the DTI data of 21 subjects. The fibers connecting two gyri were extracted for the whole brain, and categorized as short fibers only those that connect adjacent gyri. Although this work describes the presence of a high amount of short fibers, it does not present a classification of them into bundles. Only the fibers connecting two, rather large, regions are given and therefore there is no specific definition of the different SWM configurations (*i.e.* different fibers shapes and positions) within them. Although automatic placement of ROIs can ease the extraction of fibers in the whole brain, some works have also utilized this approach to study specific brain regions. This kind of studies can benefit from atlases already defined and available, and obtain a higher ROI reproducibility across subjects. For instance, in (Bozkurt et al., 2016) the authors focused in the anatomy of the supplementary motor area complex. Although the main idea of the work was to segment fibers in postmortem brains, the authors were also able to segment SWM in the pre-SMA and SMA from the tractograms of 2 subjects from the HCP database. The findings regarding the SWM unveiled a short fiber network within this functional areas, however only information about the regions they connect was given, lacking a proper bundle-based description of these fibers.

¹ <http://dsi-studio.labsolver.org>.

² <https://surfer.nmr.mgh.harvard.edu/>.

Even if automatic ROI definition facilitates group analysis in a population, the utilized templates often contain large ROIs (e.g. cortex main gyri), making difficult a fine description of the bundles. Another factor that has an impact on the results is the high cortex shape variability of the subjects (Mangin et al., 2016). Different alignment methods vary the results from the subject-template registration, and therefore the ROI delineation. Hence, this kind of approach has the disadvantage of not being as precise as the manual one, altering the definition of the bundles, especially in their perimeter.

2.1.3. Semi-automatic placement

Finally, combining manual and automatic ROI placement leads to semi-automatic definition of ROIs. There are some works that use this approach to get good results in a reasonable time. For instance, in (Vergani et al., 2014a) the authors utilized the Desikan-Killiany FreeSurfer brain parcellation (Desikan et al., 2006) for the study of the SWM fibers connecting the supplementary motor area with the precentral gyrus and Broca's area in 10 subjects from the HCP dataset. The authors manually added some exclusion regions in order to remove spurious fibers. Since this cortical parcellation is based on major gyri, the ROIs were too large, so these kind of filters allowed the authors to better delineate the bundles. They described five connections within the supplementary motor area. This study also proved the existence of fibers connecting these regions by comparing the tractography results with postmortem dissections. Another example is the work presented in (Magro et al., 2012) where the authors manually positioned 2D patches that were automatically extended to 3D patches. The 2D patches were manually drawn, based on the external traces of the pre and postcentral sulci. From them the 3D patches were constructed to cover the gray and white matter enclosed by the 2D patches. These delineations lead to a subdivision of fibers based on the combinations of different pairs of ROIs. With this processing the authors segmented 9 bundles connecting the pre and postcentral gyri. These bundle definitions are consistent with known functional areas.

Either automatic or semi-automatic approaches have the downside that, fibers connecting two ROIs often present complex configurations and different shapes. Also, large amount of outliers are segmented, especially if the regions utilized are large. These irregularities can reduce the usability of the bundles in segmentation analyses.

2.2. Fiber clustering methods

A completely different approach from ROI-based segmentation is the fiber clustering method. This class of approach is based on a fiber similarity measure. They take into account the shape and position of the fibers in order to group them into bundles, providing a disentanglement of the fibers and outliers removal. Results depend on the type of clustering and the fiber similarity measure employed. Although these approaches yield anatomically coherent bundles, they do not provide a direct reference to the cortical regions they connect (O'donnell et al., 2013) and often they have to be labeled after the grouping.

In general, fiber clustering has been widely used for the study of DWM. Thanks to their large size and low variability, those fibers can be easily analyzed. On the other hand SWM presents more complex configurations and overlapping, which makes them more difficult to reconstruct and variable across subjects. Their entanglement hinders the identification of homogeneous groups and outlier removal even with clustering methods. Despite this difficulty, in the past few years there have been some clustering-based studies focused in SWM. For instance, in (Guevara et al., 2012) the authors used an agglomerative average-link hierarchical clustering and a fiber Euclidean distance measure to group short fibers in the whole brain. The analysis was performed using a HARDI database of 12 subjects, and resulted in an atlas of 47 SWM bundles in the left hemisphere, that were then manually labeled in

function of the connected regions. The underlying study was focused in DWM, therefore the clustering was not tuned for SWM fibers. Only preliminary results and no further analyses were exposed regarding obtained short fiber bundles. A posterior refinement of this method was presented in (Román et al., 2017), adapting the clustering specifically to short fibers and removing from the analysis the long white matter bundles already identified in the same work (Guevara et al., 2012). The method was applied to the HARDI data of 74 subjects. In order to dispense with the manual labeling step, the resulting bundles were named automatically using the Desikan-Killiany FreeSurfer cortical parcellation (Desikan et al., 2006). This work described a large number of short bundles in the whole brain, which connect close gyri and also regions within the gyri.

Another work verified by means of a clustering the presence of short fibers connecting the precentral, postcentral, temporal and frontal lobes (Zhang et al., 2014). This work included into the analysis different types of diffusion-weighted data (DTI, HARDI, DSI) in order to look further how the resolution and quality of the data affects the SWM delineation. Also, they included data from human fetus and monkeys (chimpanzee and macaque) looking for the correspondence of these structures across species. In order to identify the bundles, the fibers from a subsample of the tracts were first grouped by an affinity propagation algorithm, clustering them based on their shape: close U, open U, curved line and straight line. Then to propagate this results across the rest of the tracts a k-means clustering was employed. Finally, the bundles were labeled according to the sulcal fundus they pass through. Data resolution comparison showed that DSI and HARDI data present more fibers connecting the same gyri, as well as a higher short-range connectivity. This could be due to the shape of the fibers, only able to be reconstructed using high quality data because of high curvature. Also, they found that humans present a higher amount of short fibers, which they presume might be due to their relation with the gyrification of the cortex.

In (Yeh et al., 2018) the authors clustered by means of single-link clustering both long and short fibers reconstructed from the HCP-842 SDF template using DSI studio. This template was constructed from the average of the spin distribution function of 842 subjects (in ICBM-152 standard space) from the HCP dataset, and represents an average diffusion pattern within a normal population. The clusters obtained were then labeled by neuroanatomist experts. However, the association fibers were only included into a generic category and no further information of bundle shape or the regions they connect was given. Another work, presented in (Zhang et al., 2018a), also performed a clustering for the whole brain over the data of 100 subjects from the HCP database. The aim of this study was to create a curated bundle atlas. First, the tractograms were directly aligned across subjects. Then the authors applied a group-wise spectral clustering and labeled the clusters (bundles) according to a FreeSurfer ROI atlas (Desikan et al., 2006). A second dataset composed of 584 subjects coming from different databases was conceived for segmentations purposes. Different type of subjects were considered, including data from newborn babies, autism spectrum disorder, neuropsychiatric disorders (schizophrenia, bipolar disorder and attention deficit), Parkinson disease, brain tumors and healthy subjects. The atlas results were therefore projected to the 584 subjects of the second dataset, showing a high reproducibility of the bundles. This work also described a high amount of bundles which are present in both hemispheres. Specifically regarding short fibers, 198 clusters were labeled as superficial connections in the whole brain. Although a high number of clusters was found, no specific description or validation of them was performed (this was done only for some DWM bundles).

Another work aimed at clustering the short fibers connecting the pre and postcentral gyri, using the gyri crest line (Pron et al., 2018). These are used to define the fibers that are going to be clustered. In order to do that, each line is parametrized to obtain a 1-D coordinate system as reference. The parametrization is done isometrically from the ventral to the dorsal extremity. The correspondence between the two crest lines is

ensured by aligning the hand-knob structure, which is a well-known landmark of the central sulcus. Based on the fiber extremities, those who start or end in one of the crest lines are selected. Then, these fibers were clustered by means of a k-medoids algorithm, leading to subdivisions that are functionally coherent with the homunculus.

Although fiber clustering methods are automatic and can be extended to the whole brain and a population of subjects, the parameters are difficult to tune and calculations are expensive. Some reductions of complexity can be made, for example applying the analysis to only one hemisphere, a given number of lobes, or after some filtering.

Different clustering algorithms result in a different grouping of the fibers, and for a same algorithm different parameters yield as well different bundle configurations. Usually, a fiber distance measure (e.g. Euclidean distance) is used to calculate a similarity index between fibers. A bundle can be defined for instance by choosing a maximum distance threshold (Guevara et al., 2012, 2017; Román et al., 2017; Yeh et al., 2018), or a fixed number of clusters (Zhang et al., 2018b; Guevara et al., 2017; Pron et al., 2018). However, as SWM runs continuously along the sulci and anatomy is very different from one subject to another, it is difficult to define where a bundle starts or ends. Additional difficulties stem from the fact that there are areas of the SWM that are not well reconstructed due to partial volume effect and small size. Hence, the parameters must be adapted to each data, to extract as much information as possible.

2.3. Hybrid methods

As described above, both ROI placement and fiber clustering have their advantages and disadvantages. In an attempt to bring together the advantages of both methods, hybrid approaches can help to identify anatomically meaningful bundles with well-defined shapes and present in a large population of subjects. This kind of methods in general utilize the ROIs to extract and label the fibers connecting two different anatomically meaningful regions, and to diminish the amount of fibers to be clustered, simplifying and speeding up the process. Then a clustering is applied to each group of previously extracted fibers to get bundles containing only fibers with similar shape and position within a given pair of ROIs. Clustering also helps to filtering off outliers and artifacts. Hence, the analysis takes into account the morphological information from the cortical folding patterns, and the shape and density of the fibers once they leave the cortex. Following this idea, in (Guevara et al., 2017) a FreeSurfer parcellation (Desikan et al., 2006) is applied to the tractography data of 79 subjects of a HARDI database. This parcellation was used to extract fibers with length 20–80 mm, connecting two cortical ROIs (adjacent or not). To overcome the entanglement of the fibers connecting two ROIs that are often large, a first intra-subject hierarchical clustering was applied to group fibers. This yielded groups of fibers with similar shape and position within each pair of regions (bundles). A second clustering was then performed across subjects, for keeping only the bundles present in most of the population. These results were validated by applying the method to two different groups and by automatically projecting the bundles into a third group. This was the first work using a fully automatic approach describing well-defined bundles in the whole brain, based on HARDI data.

All the methods exposed in this section, are summarized in Table 1, along with their main findings.

3. Postmortem dissections

Although tractography is the preferred method for the study of brain connections in vivo, it is susceptible to artifacts which results in many false positive and false negative fibers. A way to validate the tractography results is postmortem dissections (Catani et al., 2012, 2017; Vergani et al., 2014a, 2014b; Bozkurt et al., 2016; Burks et al., 2017; Maier-Hein et al., 2017). DWM bundles have been widely validated using this technique, as thanks to their size, position and known trajectory, they are

relatively easy to dissect. However this is not the case for SWM, since their proximity to the gray matter, variety of shapes and small size, make them more difficult to extract. Also, as mentioned before, since this kind of fibers connect two neighbor gyri (or even regions within the same gyri) by running continuously along the sulci, it is complex to identify the bundle limits regarding its neighbors. Nevertheless some validations have been made for specific brain regions as the fronto-parietal region (Catani et al., 2012), occipital lobe (Vergani et al., 2014b), and supplementary motor area (Vergani et al., 2014a; Bozkurt et al., 2016), etc. Those works showed the existence of the short association bundles in the regions they studied. These results present a great correspondence with those obtained by means of tractography, independently of the virtual dissection technique employed. Therefore, although these bundles have no specific names, the fact of being found by two different techniques gives some degree of validation of their existence, that also allows results from new works to be compared against them.

4. Registration

Group analyzes are necessary to validate the reproducibility of the results, hence subjects normalization to some common space is required. The closeness of short association fibers to the brain cortex makes them more susceptible than DWM to errors derived from brain normalization. Cortical variability across subjects is still a challenge when group analyzes are to be performed, since no perfect matching can be done across them (Mangin et al., 2016). Due to the intimate relation of the U-fibers with the cortical folding pattern, the possibility of a miss alignment is always present, especially when a simple linear transformation is used. This problem affects the fiber reproducibility studies, as they might be shifted across subjects. In (Guevara et al., 2017) a linear transformation was used to warp each subject data into Talairach space in order to perform the inter-subject analysis. Although this transformation roughly matched their data, it allowed the identification of a non-negligible number of bundles, meaning that even when they are not perfectly aligned there is a high correspondence between them, and therefore we might assume they correspond to the most stable connections. Different approaches have been used to tackle this problem, either by means of transformations over the images or direct tractogram alignment. In (Román et al., 2017) the authors performed a comparison between the results obtained from a linear and a non-linear normalization, using DTI-TK.³ Non-linear registration yielded a greater number of similar bundles, which were more homogeneous even when more restrictive similarity measures were applied. This means that non-linear registration makes possible a better matching between fibers that otherwise would be considered different. A different approach is the one performed in (Zhang et al., 2018a), where the registration method used by the authors is applied directly over the tractograms (O'Donnell et al., 2012). This kind of alignment allowed the authors not only to identify clusters belonging to known DWM bundles, but also a large number of short cortical clusters. Better alignment methods are certainly needed, ideally based on sulci and/or gyri anatomy, especially for the bundles with smaller fibers that are often the more entangled.

5. Comparison of atlases

As already mentioned before, most of the short fibers studies have been restricted to specific areas or bundles. Bundles are often represented in image volumes as probability maps, or tractography datasets. In order to compare the bundle output generated from different methods, we compared the publicly available atlases described in (Guevara et al., 2017) (*atlas1*) (Román et al., 2017), (*atlas2*) and (Zhang et al., 2018a) (*atlas3*). Some bundle examples can be seen in Fig. 1. The bundles from *atlas1* can be interactively visualized online as volumes and meshes along

³ <http://dti-tk.sourceforge.net/>.

Table 1
Superficial white matter studies and their main findings.

Paper	Data type	Regions	Main analysis	Type of analysis	Number of subjects	Connections found	Validation/Comparison
Catani et al. (2003) (Catani et al., 2003)	Tractography	Occipital and temporal gyri	Virtual dissection of the tracts connecting two ROIs	Manual ROI placement	11 DTI (averaged)	Chain of U-shaped fibers running laterally to the inferior longitudinal fasciculus that connect adjacent gyri of the lateral occipito-temporal region	
Wakana et al. (2004) (Wakana et al., 2004)	Tractography	Whole brain	Virtual dissection of the tracts	Manual ROI placement	4 DTI	Tracts in the frontal area, close to the SLF, a tract in the occipital lobe (VOF)	
Oishi et al. (2008) (Oishi et al., 2008)	Tractography	Whole brain	Virtual dissection of the tracts connecting two ROIs (from atlas average of 81 subjects)	Automatic based on ROI atlas	10 DTI	SF-IF, MF-PrC, PrC-PoC, SP-parieto/temporal regions (SM and An)	
Zhang et al. (2010) (Zhang et al., 2010)	Tractography	Whole brain	Multi-ROI approach to reconstruct tracts of interest	Automatic ROI warping	20 DTI	SP-PoC, SP-An, SP-PrCu, SP-SO, SP-MO, SP-SM, Ci-SF, Ci-PrCu, SF-MF, SF-IF, SF-PrC, MF-IF, MF-PrC, IF-PrC, PrC-PoC, PoC-SM, An-MO, An-SM, Cu-Li, Cu-SO, Cu-MO, Fu-IO, FU-MO, SO-MO, IO-MO, ST-MT, ST-SM, IT-MT, LOF-MOF	Comparison between manual and automated ROI placement
Catani et al. (2012) (Catani et al., 2012)	Tractography	Left frontal lobe, central, pre-central, perinsular and fronto-marginal sulci	Virtual dissection of the tracts connecting two ROIs	Manual ROI placement	1 and 12 HARDI	Frontal lobe: SF-IF (FAT), SF-MF, PrC-MF, Posterior/anterior orbitofrontal-polar cortex (FOP), posterior precentral cortex - anterior prefrontal cortex (FSL, FIL), FMT. PrC-PoC: paracentral, hand superior, hand middle, hand inferior, face superior and face inferior. Ins-Or/Tr/Op/PrC/SuC.	Postmortem dissections
Magro et al. (2012) (Magro et al., 2012)	Tractography	Pre and post-central gyri	Each region subdivided into 3 ROIs, used as seed regions	Semi-automatic ROI placement	20 DTI	PrC-PoC: 9 bundles per hemisphere (resulting from the combination of the 6 ROIs)	
Guevara et al. (2012) (Guevara et al., 2012)	Tractography	Left hemisphere (symmetrized to the right hemisphere)	Clustering (hierarchical) and manual labeling using gyral parcellation	Semi-automatic, clustering and manual labeling	12 HARDI	SF-IF (ant, mid and post), SF-MF (ant, mid and post), MF-IF, MF (mid, mid2, post, post2), IF-Ins, IF (post, inf), LFO (inf, sup), MFO, MFO-Ci, SF-Ci (mid), MF-PrC (sup, mid), PrC-PoC (sup, inf), PrC-Ins, PrC-SM, PaC-PrCu, PoC-SM, SM, SP, An (sup, inf), ST-An, MT-An, ST (post), MT-Ins, ST-Ins, IT-MO, Cu, Cu-Li, Li, Fu (ant, mid, post), PrCu-Ci, PrCu-SF, Ci (ant, mid, post)	
Vergani et al. (2014) (Vergani et al., 2014a)	Tractography	SMA, IF gyrus, caudate nucleus, PrC y Ci gyri	Whole brain tractography segmented into tracts connecting two ROIs	Semi-automatic ROI placement	10 from HCP 12 for dissection	SMA-PrC, SMA-Ci, SMA-Op (FAT), SMA-Striatum, SMA callosal fibers	Postmortem dissections
Zhang et al. (2014) (Zhang et al., 2014)	Tractography	Neighboring gyri coursed around by cortical major sulci (CS, PrS, PoS, STS, IFS, IPS, ITS, SFS, LOS, TOS)	Fiber clustering, fiber extraction and labeling based on sulci	Semi-automatic, expert manual labeling (Connecting ROIs)	18 human DTI 10 human HARDI 68 from HCP 2 human DSI 21 human fetus DTI 15 chimpanzee DTI 12 macaque DTI	In the three modalities: SF-MF, MF-IF, PrC-PoC, left SP-IF and right PoC-SP. DSI: MF-IP left SF-IP, MF-SM, IF-MT, PoC-IP, SP-SM, SM-MT, MT-IT, IP-MO; right SF-SP, MF-MT, IF-SP, PrC-SP, SP-IP, SP-SO, SP-MT, ST-MT. HARDI: SP-SM, MF-MT, SF-IF, SO-MO, MF-PrC; left PoC-SM, SP-MT, ST-MT; right SP-IP, SM-PrC, IP-SM, IP-MT. DTI: SF-IF, MF-PrC, IF-PrC, SM-MT, PrC-SP; left SF-PrC, SF-PoC, SF-SP, PrC-MT, SP-SO, IP-MT, IF-ST, PoC-IP; right PrC-IP, PoC-IP, IP-MO, SM-MO, ST-SM.	Co-localization patterns over DTI, HARDI and DSI data of human, chimpanzee (DTI) and macaque (DTI) brains. Verification of the existence of fibers, and preservation of U-shape
Vergani et al. (2014) (Vergani et al., 2014b)	Postmortem	Right hemisphere occipital lobe	Postmortem dissection	Manual ROI placement	3	Cu-PrCu, upper-lower edges of calcarine cortex (Cu-Li), upper-lower parts of Cu, sup/mid/inf occipital sulcus, sup-ant occipital lobe, Fu-Li	Is a Postmortem study
Rojkova et al. (2015) (Rojkova et al., 2016)	Tractography	Frontal lobe	Virtual dissection of the tracts connecting two ROIs	Manual ROI placement	47 HARDI	PrC-PoC: Paracentral, hand superior, middle and inferior, face. FAT, 5 fronto-insular bundles, FSL, FIL, FOP, FMT	Verified by Catani et al. (2012)
Wu et al. (2016) (Wu et al., 2016)	Tractography	Temporo-parieto-occipital region	Virtual dissection of the tracts	Manual ROI placement	10 DSI	Posterior part of MT and IF with An and SM (Posterior segment of the FSL), IP with lower temporal and occipital lobe (VOF); IT, MT, Fu and IO with SP	Postmortem dissections

(continued on next page)

Table 1 (continued)

Paper	Data type	Regions	Main analysis	Type of analysis	Number of subjects	Connections found	Validation/Comparison
Bozkurt et al. (2016) (Bozkurt et al., 2016)	Tractography and postmortem	SMA in both hemispheres	connecting two ROIs Virtual dissection of the tracts using ROIs (DSI studio)	Automatic ROI placement	10 postmortem 1 cadaveric head 2 from HCP	Connections of the pre-SMA with the prefrontal cortex, pre-SMA with the SMA proper, the SMA proper with the precentral region (motor cortex) and the pre-SMA/SMA proper with the pars Opercularis/ Traingularis (frontal aslant tract)	Postmortem dissections
Burks et al. (2016) (Burks et al., 2017)	Tractography	Parietal lobule of both hemispheres	Virtual dissection of the tracts using ROIs (DSI studio)	Automatic ROI placement	10 from HCP 10 post-mortem	SM-An, SM-SP, SM-Primary sensory cortex, An-SP	Post-mortem dissections
Ouyang et al. (2016) (Ouyang et al., 2017)	Tractography	Whole brain	Virtual dissection of fibers connecting two gyri	Automatic ROI placement	21 healthy DTI	No specific bundles, short fibers are grouped depending on the two adjacent gyri they connect.	
Catani et al. (2017) (Catani et al., 2017)	Tractography	Parietal lobe	Virtual dissection of the tracts connecting two ROIs (startrack and trackvis)	Manual ROI placement	21 human		
6 macaque	SP-SM, SP-An, PoC-SM, PoC-An, SP-PoC, SM-An						
Intra-parietal U-fibers: Anterior SM-Posterior SM, anterior-intermediate-posterior PrCu, Regions of the SP	Postmortem dissections						
Guevara et al. (2017) (Guevara et al., 2017)	Tractography	Whole brain	Fiber extraction and labeling from ROIs, followed by a clustering	Automatic ROI placement and fiber clustering	79 HARDI	Both hemispheres: CAC-PrCu_0, CMF-PrC_0, CMF-PrC_1, CMF-RMF_0, CMF-SF_0, IC-PrCu_0, IP-IT_0 IP-MT_0, IP-SM_0, IP-SP_0, LOF-RMF_0, LOF-RMF_1, LOF-ST_0, MOF-ST_0, MT-SM_0, MT-ST_0, Op-Ins_0, Op-PrC_0, Op-SF_0, Or-Ins_0, PoCi-PrCu_1, PoCi-RAC_0, PoC-PrC_0, PoC-PrC_1, PoC-PrC_2, PoC-SM_0, PrC-Ins_0, PrC-SM_0, RMF-SF_0, RMF-SF_1, SM-Ins_0, SP-SM_0, ST-TT_0, Tr-Ins_0, Tr-SF_0. Left Hemisphere: CMF-Op_0, CMF-PoC_0, Fu-LO_0, IP-LO_1, IP-SP_1, IT-MT_0, LOF-Or_0, PoC-Ins_0, PoCi-PrCu_0, PoCi-SF_0, PoC-PrC_3, PoC-SM_1, PrC-SF_0, RAC-SF_1, ST-Ins_0. Right hemisphere: CAC-PoCi_0, CMF-SF_1, Cu-Li_0, Fu-LO_1, IP-LO_0, IT-MT_1, IT-MT_2, LOF-MOF_0, LO-SP_0, Op-Tr_0, PoCi-PrCu_2, PoC-SP_0, PrC-SP_0, RAC-SF_0.	Between group atlas comparison, bundle segmentation and comparison with the literature
Román et al. (2017) (Román et al., 2017)	Tractography	Whole brain	Clustering (hierarchical) and automatic labeling based on gyri	Automatic clustering and ROI labeling	74 HARDI	Both hemispheres: SP_SP_0i, PreC_SF_0i, PoC_Prec_3i, Op_SF_0i, CMF_Prec_0i, PoC_Prec_1i, MT_MT_0i, PreC_SM_1i, CMF_CMF_0i, Fu_IT_0i, IP_SP_0i, MT_ST_0i, LorF_LorF_0i, LO_LO_0i, CMF_Op_0i, RoMF_SF_1i, Tr_SF_0i, SM_SM_2i, SM_SM_0i, RoMF_RoMF_1i, PoC_SM_0i, PoC_Prec_2i, PoC_Prec_0i, MT_MT_1i, CMF_Prec_1i, Fu_Fu_0i, PreC_SM_0i, ST_ST_0i, Tr_RoMF_0i, LO_LO_1i, RoMF_SF_0i, RoMF_RoMF_0i, SM_SM_1i Left: IT_IT_1i, SF_SF_0i, Fu_Fu_1i, IT_IT_0i, PreC_Prec_0i, ST_ST_1i, Cu_Lg_0i, PreCu_Precu_0i, MT_MT_1i, LO_LO_2i, PreC_Ins_0i Right: Tr_Tr_0r, Tr_Ins_0r, MT_MT_0r, SF_SF_2r, RoMF_SF_0r, RoMF_RoMF_0r, RoMF_RoMF_1r, PoC_PoC_1r, PoC_Prec_1r, SP_SP_0r, PreCu_Precu_0r, SF_SF_1r, IP_LO_0r, IP_IP_0r, LorF_LorF_1r, Tr_SF_1r.	Bootstrap strategy, bundles segmentation and comparison against another atlas
Jung et al. (2017) (Jung et al., 2017)	Tractography	Frontal lobe, parietal and temporal lobes	Virtual dissection of the tracts	Automatic and manual	24 subjects	Extratemporal lobe: PH _a -SP _{7m} , ST _m -IP _{pfcm} , MT _m -IP _{pfcm} , PH _m -SP _{7m} , ST _p -IP _{pfop.pj.pjcm} , MT _p -SP-7pc/IPS _{ips1} /IP _{pfop.pjt.pj.pjm.pjcm.pga.pgp} , IT _p -SP _{7pc} /IP _{pfcm} .	

(continued on next page)

Table 3
Bundles common to the three atlases.

ID	left									ID	right								
	A1	A2	A3	A1/ A2	A2/ A1	A1/ A3	A3/ A1	A2/ A3	A3/ A2		A1	A2	A3	A1/ A2	A2/ A1	A1/ A3	A3/ A1	A2/ A3	A3/ A2
L1	lh_CMF- Op_0	lh_CMF_Op_0i	c_00298_lh	1,00	0,97	0,99	0,96	0,84	0,95	R1	rh_CMF- PrC_0	rh_CMF_PreC_0i	c_00293_rh	1,00	0,88	1,00	0,98	0,99	1,00
			c_00205_lh			0,99	0,90	0,84	0,89	R2	rh_CMF- PrC_1	rh_CMF_PreC_1i	c_00338_rh	1,00	0,89	0,87	0,91	0,92	0,98
			c_00375_lh			1,00	0,99	1,00	1,00	1,00	R3	rh_CMF-SF_1	rh_CMF_CMF_0i	c_00259_rh	0,99	0,98	1,00	0,97	0,82
L2	lh_Op-SF_0	lh_Op_SF_0i	c_00300_lh	1,00	1,00	0,93	1,00	0,97	1,00	R4	rh_Fu-LO_1	rh_Fu_Fu_0i	c_00401_rh			0,97	0,95	0,90	0,99
			c_00359_lh			0,90	0,92	0,99	0,98	R5	rh_IP-LO_0	rh_LO_LO_0i	c_00076_rh	1,00	0,92	1,00	0,82	0,97	1,00
			c_00322_lh			0,86	1,00	0,82	1,00	R6	rh_IP-SM_0	rh_SM_SM_0i	c_00430_rh	1,00	0,92	1,00	0,93	0,93	0,94
L3	lh_CMF- SF_0	lh_CMF_PreC_0i	c_00293_lh	1,00	0,82	0,99	0,83	0,93	1,00	R7	rh_SP-SM_0	rh_SP_SP_0i			0,99	0,90	0,90	0,95	0,98
			c_00278_lh			0,99	0,84	0,94	0,97				c_00458_rh	1,00	0,99	0,99	0,93	0,99	0,98
			c_00076_lh	1,00	0,90	1,00	0,98	0,95	0,99				c_00362_rh			0,88	0,84	0,80	0,99
L4	lh_IP-LO_1	lh_LO_LO_0i	c_00076_lh	1,00	0,90	1,00	0,98	0,95	0,99						0,98	0,84	0,80	0,99	
L5	lh_IP-SP_1	lh_IP_SP_0i	c_00450_lh	1,00	0,93	1,00	0,88	0,93	0,98		rh_IP-SP_0	rh_IP_SP_0i	c_00017_rh	1,00	1,00	0,98	0,84	0,91	0,88
L6	lh_MT-ST_0	lh_MT-ST_0i	c_00119_lh	1,00	0,83	1,00	0,87	0,93	0,89	R8			c_00042_rh			0,95	0,92	0,96	0,92
			lh_ST-ST_0i	1,00	0,85			0,96	0,91				c_00059_rh			0,91	0,91	0,85	0,91
L7	lh_PoC- SM_1	lh_SP_SP_0i	c_00362_lh	1,00	0,84	1,00	0,98	0,86	0,98			rh_SP_SP_0r	c_00046_rh	0,98	0,86	0,90	0,92	0,97	0,94
L8	lh_SP-SM_0		c_00458_lh	1,00	1,00	1,00	0,85	0,96	0,93	R9	rh_IT-MT_1	rh_MT_MT_1i	c_00744_rh	1,00	0,93	1,00	0,95	1,00	0,98
L9	lh_PoC- PrC_2	lh_PoC_PreC_2i	c_00303_lh	1,00	0,92	1,00	0,99	0,85	1,00	R10	rh_LO-SP_0	rh_IP_LO_0r	c_00084_rh	1,00	0,91	1,00	0,87	0,85	1,00
L10	lh_PoC- SM_0	lh_SM_SM_2i	c_00337_lh	0,99	0,99	0,88	0,80	0,94	0,94				c_00064_rh			1,00	0,99	0,82	0,99
			lh_PreC_SM_0i	1,00	0,97			0,82	0,87				c_00062_rh			0,96	1,00	0,85	1,00
			c_00201_lh			0,92	0,85	0,91	1,00				c_00036_rh			0,99	0,85	0,87	1,00
L11	lh_Tr-SF_0	lh_Tr_SF_0i	c_00591_lh	0,89	0,99	0,86	0,94	0,92	0,94	R11	rh_MT-SM_0	rh_MT_ST_0i	c_00455_rh	0,96	0,83	1,00	0,86	1,00	0,97
			c_00607_lh	1,00	1,00	0,93	0,82	0,95	0,87	R12	rh_MT-ST_0	rh_ST-ST_0i	c_00440_rh			1,00	0,91	0,94	0,95
L12	lh_RMF- SF_0	lh_RoMF_SF_0i	c_00642_lh	1,00	0,99			0,87	0,89	R13	rh_Op-SF_0	rh_Op_SF_0i	c_00322_rh	0,99	1,00	0,93	1,00	0,96	1,00
						0,81	0,97	0,97	1,00				c_00359_rh			0,92	0,99	0,94	0,96
												c_00300_rh			0,98	1,00	0,97	1,00	
												rh_CMF_Op_0i		1,00	1,00		0,86	1,00	
												c_00375_rh				0,91	0,99	0,99	
												c_00267_rh				0,85	1,00	0,93	
										R14	rh_PoC- PrC_1	rh_PoC_PreC_2i	c_00412_rh	1,00	0,97	1,00	0,93	0,97	0,95
										R15	rh_PoC- PrC_2	rh_PoC_PreC_3i	c_00296_rh	1,00	0,96	1,00	0,82	0,97	0,93
												c_00391_rh				1,00	0,95	0,97	
												c_00398_rh				1,00	0,95	0,90	
										R16	rh_PrC-SM_0	rh_PreC_SM_0i	c_00201_rh	1,00	0,96	0,99	0,94	0,92	1,00
										R17	rh_PoC-SM_0			1,00	0,87	0,99	0,82	0,92	1,00
												rh_PoC_SM_0i		1,00	0,98		0,93	1,00	
										R18	rh_PoC-SP_0	rh_PoC_PoC_1r	c_00458_rh	1,00	0,99	0,99	0,86	0,91	0,85
												c_00422_rh				0,95	0,88	0,81	
										R19	rh_RMF-SF_0	rh_RoMF_SF_1i	c_00589_rh	1,00	0,99	0,95	0,81	0,96	0,98
												c_00661_rh			0,93	0,96	0,80	0,95	
												rh_Tr_SF_0i		1,00	0,99		0,92	0,92	
												c_00629_rh				0,81	0,84	0,87	
												c_00607_rh				0,88	0,86	0,95	
										R20	rh_RMF-SF_1	rh_RoMF_SF_0r	c_00368_rh	1,00	0,98	1,00	1,00	0,97	1,00
												c_00405_rh				1,00	1,00	0,91	
										R21	rh_Tr-SF_0	rh_Tr_SF_1r	c_00645_rh	0,99	1,00	0,87	0,95	0,94	0,98

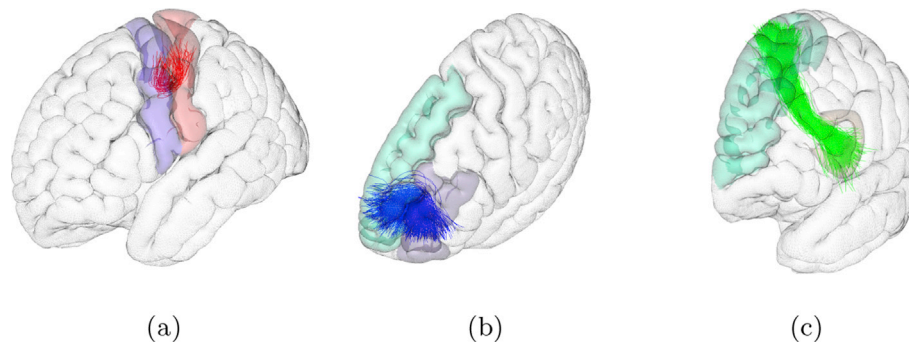
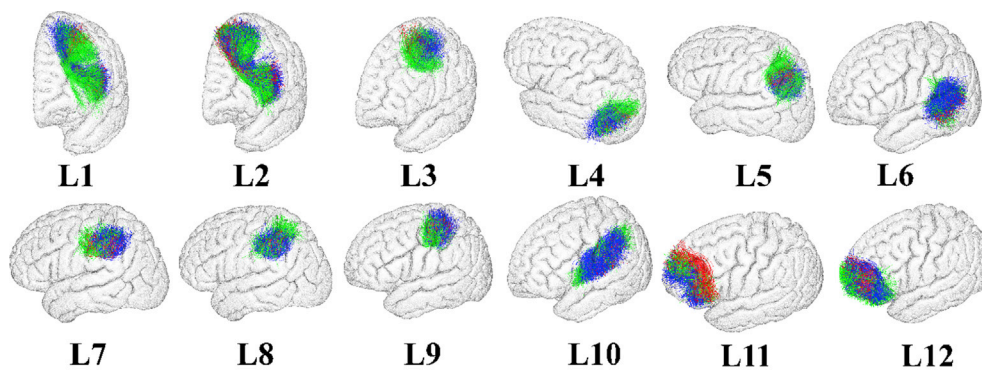
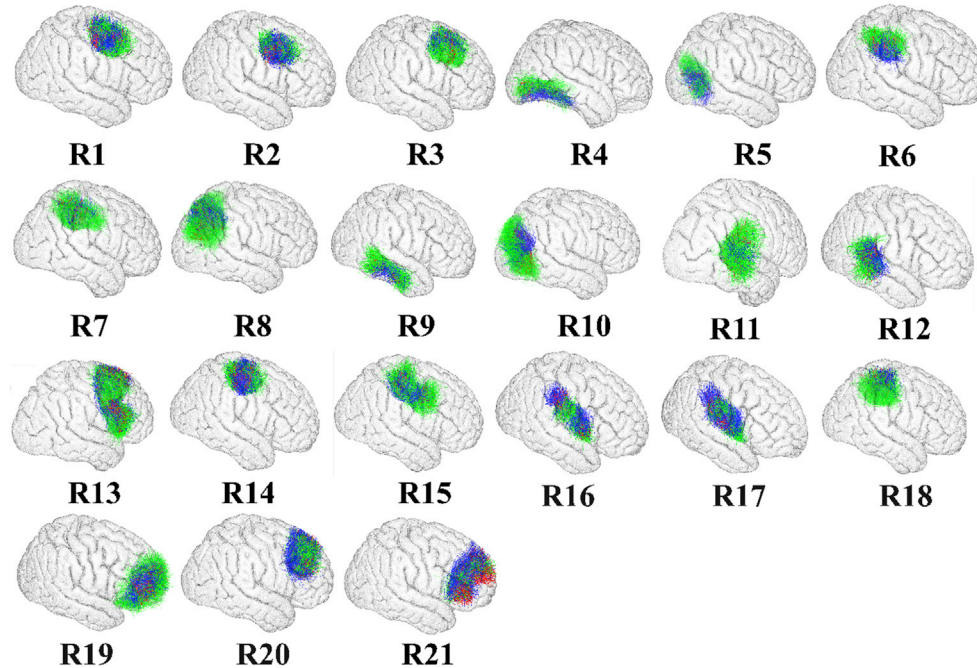


Fig. 1. SWM bundles of fibers connecting different gyri of the left frontal region. These structures can connect adjacent gyri (showing their characteristic close U-shape) or skip one or more sulci (open U-shape). (a) SWM bundle from *atlas1* connecting pre and postcentral gyri, (b) SWM bundle from *atlas2* connecting rostral middle frontal and superior frontal gyri and (c) SWM cluster from *atlas3* connecting pars opercularis and superior frontal gyri.



(a) Bundles common to the three atlases in the left hemisphere



(b) Bundles common to the three atlases in the right hemisphere

Fig. 2. Bundles common to the three analyzed atlases. In red the bundles belonging to *atlas1*, in blue the bundles belonging to *atlas2* and in green the bundles of *atlas3*.

present the average percentage of all the similar bundles in the atlas and its standard deviation.

In most cases, several bundles from *atlas3* correspond to one from *atlas1* and *atlas2*. These two last atlases present a one to one

relationship between them for most of the bundles, most likely because they come from the same database. Both atlases (*atlas1* and *atlas2*) present some gaps in the brain less covered by short bundles, specially in temporal and occipital regions, since most of the bundles are present

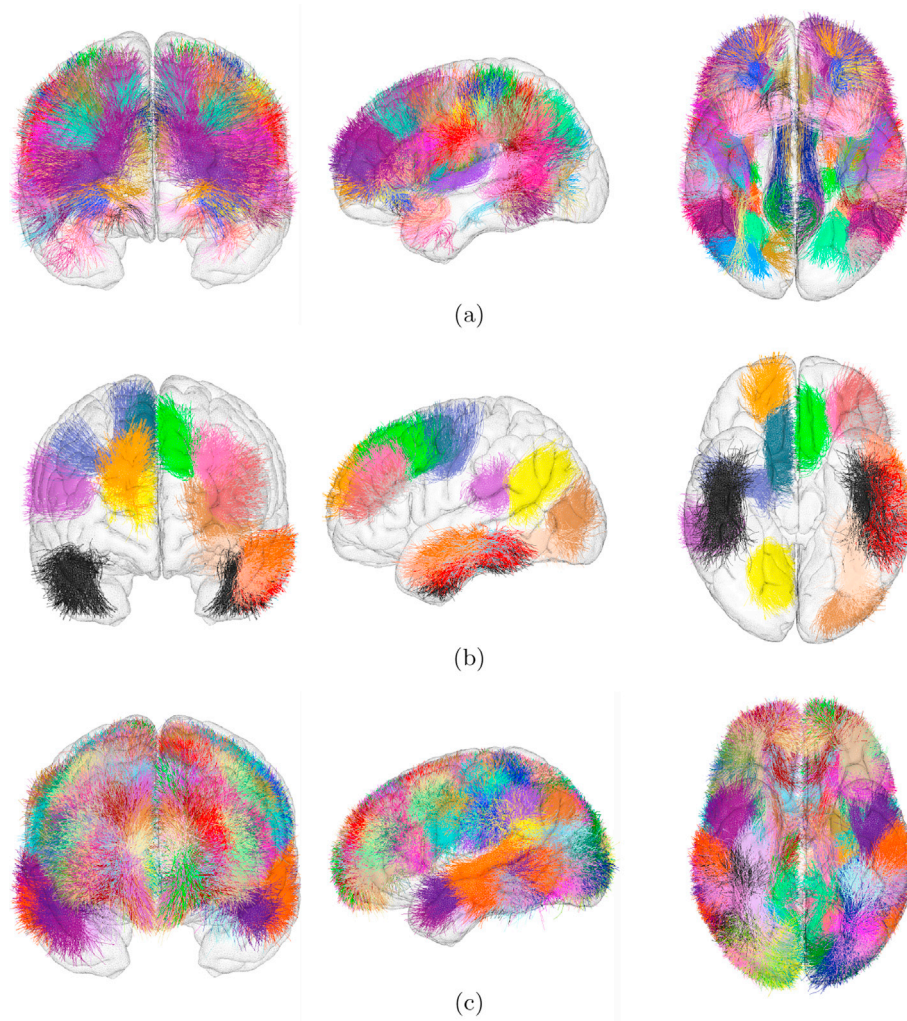


Fig. 3. Compilation of distinctive SWM bundles from the three analyzed atlases. (a) all the bundles from *atlas1*, (b) bundles from *atlas2* that are not present in *atlas1*, and (c) bundles from *atlas3* that are not in *atlas1* or *atlas2*.

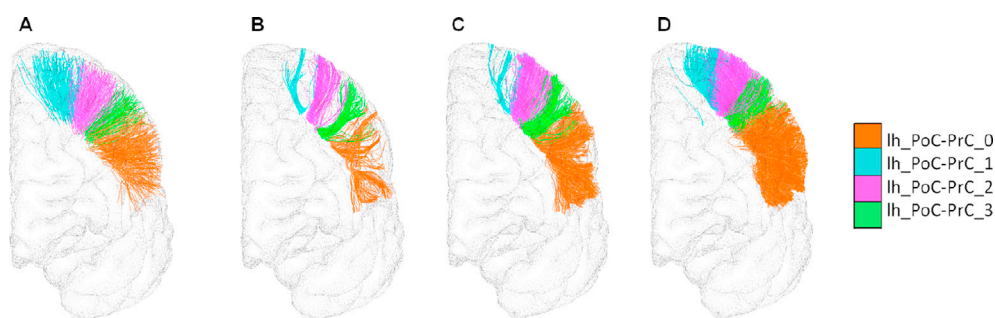


Fig. 4. A: Bundles connecting pre and postcentral gyri in the *atlas1* (PoC-PrC 0,1,2 and 3). B, C and D present the segmentations from one subject tractography data generated using DTI, GQI and MRtrix, respectively.

in the fronto-parietal region. We provide a compilation of the distinctive bundles from the three atlases. The selection was based on the connectivity criteria used to define the bundles for each atlas. *Atlas1* used the most restrictive method, since the bundles were constructed with fibers connecting pairs of specific regions, i. e. 100% of the fibers of a bundle connected two regions of Desikan-Killiany atlas in all the subjects. Hence, all the bundles of this atlas were selected and are displayed in Fig. 3a (100 bundles). Next, *atlas2* used a minimum connectivity criterion of 50% of the fibers connecting a pair of defined regions (also based on Desikan-Killiany atlas). Hence, we selected the

bundles present in *atlas2* that were not identified in *atlas1*, displayed in Fig. 3b (17 bundles). A main difference between *atlas1* and *atlas2* is that *atlas2* includes intra-gyri bundles which are not detected by *atlas1* method. Also, as *atlas2* method used non-linear registration, some extra bundles were detected connecting adjacent gyri. On the other hand, *atlas3* was constructed from a superior quality database (HCP) (HCP Young Adult, 1200), with higher spatial resolution and a multi-shell acquisition, which increases the amount of tractable short fibers and the possibility to disentangle large U-fiber bundles into smaller clusters. Besides, this allowed the authors to find a big amount of fiber clusters

all over the brain. Fig. 3c shows the clusters in *atlas3* that are not present in *atlas1* or *atlas2* (96 bundles). We can observe that a large amount of SWM bundles are obtained, covering all locations within the brain (Fig. 3c). Note that clusters in *atlas3* are smaller than clusters in *atlas1* and *atlas2*. Also, as mentioned above, among the bundles of *atlas3*, we can find bundles covering the regions covered by the other atlases, but, in general, with smaller clusters, and different degree of overlapping. Indeed, as our criterion for comparing clusters was very restrictive (with a minimum of 80% of similarity between fibers), several clusters in Fig. 3c presents a degree of overlapping with bundles in *atlas1* and *atlas2*. Hence, the set of bundles shown in Fig. 3a, b and 3c is a representative compilation of SWM bundles present in the most recent SWM bundle atlases (in MNI space).⁷ Table A.8 lists all the bundles for the left hemisphere (109 bundles) and Table A.9 lists all the bundles for the right hemisphere (104 bundles). The regions connected by bundles selected from *atlas3* were determined using the Desikan-Killiany cortex parcellation in MNI space, calculated from the ICBM152 template.(see Fig. 1 and Fig. 2)

6. SWM bundle reproducibility and dMRI parameter configuration

Few studies have evaluated the sensitivity of superficial white matter bundle segmentation to diffusion local model and tractography methods. Several aspects in the dMRI processing pipeline can affect the SWM reconstruction. For example, the white matter propagation mask used by the tractography algorithms to define the fiber space. The voxels in the periphery of the white matter mask are affected by partial volume effect, and can be erroneously excluded from the mask, producing a reduction of the reconstructed SWM fibers (Guevara et al., 2011). Hence a very low FA threshold is recommended, or a mask based on T1 image. A recent work performed a study of the effect of the number of fibers in tractography reconstruction of white matter bundles (Román et al., 2019). Using a subject of the HCP database (HCP Young Adult, 1200) the authors found that probabilistic tractography, based on constrained spherical deconvolution (Tournier et al., 2007), calculated using MRtrix software⁸ lead to a better reconstruction of some SWM bundles than deterministic tractography based on Generalized Q-sampling Imaging (GQI) (Yeh et al., 2010) using DSI Studio software. The study also found that SWM bundles are more sensitive to the number of fibers used in tractography than DWM bundles. A value of 1.5M fibers was found to be adequate for DSI Studio and 3M fibers for MRtrix. The sensitivity to other parameters was not quantitatively evaluated, but a set of parameters for both softwares was empirically tuned for SWM reconstruction (listed below).

We extended this evaluation to the compilation of SWM bundles from the three atlases, described in section 5 and listed in Tables A.8 and A.9 (Fig. 3). For the analysis, we used multi-shell diffusion MRI of 50 subjects of the Human Connectome Project (HCP) database (HCP Young Adult, 1200), from the 1200 Subjects Data Release (S1200 Data). The dMRI data was collected over three b-values (1000, 2000, 3000 s/mm^2), with an isotropic voxel size of 1.25mm. We worked with the HCP pre-processed data (Glasser et al., 2013), where diffusion imaging distortion corrections were applied (Andersson et al., 2003; Andersson and Sotiropoulos, 2015). Diffusion data is aligned to the native structural space.

We calculated whole brain tractography in the subject space, for different numbers of fibers, using DSI Studio, based on the Generalized Q-sampling Imaging (GQI) (Yeh et al., 2010) method. Deterministic tractography algorithm (Yeh et al., 2013) was applied using the following parameters: angular threshold = 90°, step size = 0.25mm, minimum length = 30mm, maximum length = 250mm, smoothing = 0.5, and QA threshold = 0. Datasets were calculated for 500k, 1M, 1.5M and 2M streamlines. Furthermore, using the same parameters, the tractographies

were also calculated based on DTI model, using DSI Studio.

We also calculated tractographies using MRtrix, based on constrained spherical deconvolution model (Tournier et al., 2007) (IFOD2). Probabilistic tractography (Christiaens et al., 2015) with Anatomically-Constrained Tractography (ACT) (Smith et al., 2012) was calculated, using a step size = $0.1 * \text{voxelsize}$, angle threshold = 90°, minimum length = 30mm, maximum length = 250mm and cutoff value = 0.06. Finally, a Spherical-deconvolution Informed Filtering of Tractograms (SIFT) (Smith et al., 2013) was applied, keeping the 10% of the fibers. Final datasets of 1M, 2M, 3M, and 5M streamlines were calculated.

Then, an automatic WM bundle segmentation algorithm (Labra et al., 2017) was applied to each dataset to extract the bundles included in the compilation of SWM atlas bundles described above and listed in Tables A.8 and A.9. The algorithm calculates a distance between each fiber of the atlas and each fiber of the subject's tractography. It uses the maximum Euclidean distance between corresponding points of the two fibers, normalized by the difference between the length of the atlas fiber and the fiber of the subject (d_{me}). Before this processing, the fibers were transformed to MNI space, by applying the non-linear transformation from structural to MNI152 space, calculated with FNIRT software (Andersson et al., 2007), provided with the HCP database. The segmentation algorithm uses a distance threshold parameter, that was set between 6 and 8mm for deterministic tractography, according to the bundle length (Román et al., 2017). In the case of MRtrix, with probabilistic tractography, fibers have more irregular trajectories, hence higher thresholds, between 8 and 10mm, were used.

A first analysis evaluated the difference between the segmentation results using different number of fibers, based on a fiber similarity measure, as described in (Román et al., 2019). The tests were conducted for the three local diffusion model/tractography configurations: DTI and deterministic tractography with DSI Studio (called DTI), GQI and deterministic tractography with DSI Studio (called GQI), and IFOD2 and probabilistic tractography using ACT + SIFT with MRtrix (called MRtrix). The comparison was performed between the dataset with more fibers and the remaining datasets, separately for each configuration. We calculated the percentage of fibers reconstructed for each smaller dataset, and observed a saturation trend for the maximum number of fibers. The comparison confirmed that 1.5M fibers for GQI and 3M fibers for MRtrix are sufficient to obtain about a 95% of fiber similarity with respect to the maximum tested value (2M and 5M fibers, respectively), without any visual difference between the segmented bundles and also no significant difference when comparing bundle masks with 1.25mm of resolution. For DTI, a number of 1.5M was found to be appropriate, with a 97% of fiber reconstruction with respect to 2M fibers.

Next, we evaluated the reproducibility and variability of the SWM bundles across the 50 subjects for the three local diffusion model/tractography configurations (DTI, GQI and MRtrix). For that, we calculated the percentage of bundles successfully reconstructed from the total of subjects (R). A minimum of five fibers was considered to count a bundle as reconstructed in a subject. Also, we calculated the relative standard deviation of the number of fibers (RSD) to have an insight into the variability of the bundles. Tables A.8 and A.9 list the reproducibility and variability results for the left and right hemispheres respectively, associated to the bundle name, the connected regions and the atlas the bundle belongs to. The bundles are sorted in descending order of reproducibility and increasing order of variability. That is, the bundles are listed according to their stability, from highest to lowest. Note that bundle variability (standard deviation of the number of fibers RSD) is very similar in DTI and GQI, but is lower for MRtrix. Bundle reproducibility is higher and with a value of 100% in all the bundles for MRtrix and lower for the other methods, being very low for some bundles using DTI. However, there are about 40 bundles per hemisphere that are very stable for all the methods, with a reproducibility superior to 95%. Another aspect to consider is the coverage of the segmented bundles with respect to the atlas bundle. Fig. 4 illustrates the segmentation results of one subject, for

⁷ available upon request to. mguevara.bme@gmail.com

⁸ <http://www.mrtrix.org/>.

Table 4
SWM clinical studies using diffusion-weighted imaging.

Paper	Data type	Type of application	type of analysis	Regions	Type of bundle identification	Number of subjects	Results found
Sundaram et al. (2008)	Tractography	SWM in autism	DTI-derived metrics (ADC and FA) and fiber length	Frontal lobe	Manual delineation of 50 ROIs	50 children patients 16 controls	ADC significantly higher in ASD group. FA significantly lower in ASD.
Shukla et al. (2011)	Voxel	SWM in autism	DTI-derived metrics (MD, RD and FA)	Frontal, parietal and temporal lobes in both hemispheres	SWM mask from FA skeleton	24 controls 26 patients DTI	Children with ASD presented and increased MD and RD of SWM in frontal, temporal and parietal lobes of both hemispheres. FA was reduced in bilateral frontal lobes
Phillips et al. (2011)	WM mesh	SWM and schizophrenia	DTI-derived metrics (FA)	Whole brain	No bundle identification	150 including patients and their relatives	Reduced FA in the left temporal and bilateral occipital regions of the patients
Malykhin et al. (2011)	Voxel	SWM changes in age	DTI-derived metrics (AD, RD)	Prefrontal white matter	Manual parcellation of WM using ROIs	69 aged 22-84	Increase in the AD and RD with age starting from the 60s
Catani et al. (2013)	Tractography	Verbal fluency in aphasia	Bundle lateralization	Frontal	Manual segmentation of fibers connecting two ROIs	35 patients 29 controls	FAT (connecting Broca's region with the anterior cingulate and Pre-SMA) left lateralized in right-handed. FAT correlated to verbal fluency.
Nazeri et al. (2013)	Voxel	SWM in schizophrenia	DTI-derived metrics (FA)	Whole brain	SWM mask and TBSS	44 patients 44 controls	Reduced FA in 5 SWM clusters (cortex): Superior lateral occipital, PrCu, PC, MF and IF, Orbitofrontal cortex, precentral, insula operculum, frontal operculum.
Phillips et al. (2013)	WM mesh	SWM relation with age, sex and hemisphere	DTI-derived metrics (FA, RD and AD)	Whole brain	No bundle identification	65 aged 18–74 years	Decrease of FA related to age, as well as an increase of AD and RD, and also a leftward asymmetry
Gao et al. (2014)	Tractography and fMRI	Relevance of SWM in Alzheimer	DTI-derived metrics (AD) and fMRI	Whole brain	ROIs from regions activated in prospective memory task (4 mm < fibers <35 mm)	13 young 13 healthy 17 patients	Short fibers more vulnerable to aging (less myelinated). MD correlated (+) with fMRI signal change and (-) with efficiency in prospective memory performance.
Hatton et al. (2014)	Tractography	SWM in early Psychosis	DTI-derived metrics (FA)	Insula-temporoparietal junction	13 SWM bundles obtained by using ROIs as seed	42 patients 45 controls	Reduced FA in the bundle connecting the superior temporal and middle temporal gyri
Wu et al. (2014)	WM mesh	SWM development in children and adolescents	DTI-derived metrics (FA, AD, RD, MD)	Whole brain	WM parcellation template	133 aged 10–18 years	Increased FA and decreased MD and RD beneath bilateral motor sensory cortices and superior temporal auditory cortex, as well as an increase in FA and AD in bilateral orbitofrontal regions and insula
Nazeri et al. (2015)	Tractography	SWM in Alzheimer	DTI-derived metrics (FA)	Whole brain SWM	SWM skeletonized probabilistic map, obtained from ROI masks (MNI atlas of cortical structures) and TBSS (automatic)	141 healthy	Inverse relationship of FA and age decline in tracts: right superior frontal sulcus tract, left superior frontal sulcus tract, right orbito-polar tract, right sub-intra-occipital tract, right sub-precuneal tract, left sub-parieto-occipital tract, left sub-intra-parietal tract
Ecker et al. (2016)	Tractography	SWM and gyrification in ASD	DTI-derived metrics (AD)	Whole Brain	3D ROIs from clusters of increased gyrification (fibers <30 mm)	51 patients 48 controls	Tracts originating/terminating in clusters of increased gyrification showed increased AD
Reginold et al. (2016)	Tractography	SWM in Alzheimer	DTI-derived metrics (MD, RD, AxD, FA)	Frontal and parietal, temporal and occipital lobes	Manual segmentation of fibers	16 patients 24 controls	Increased MD, RD and AxD in fibers in the temporal lobe
Phillips et al. (2016a)	WM mesh	SWM abnormalities in Huntington's disease	DTI-derived metrics (AD, RD)	Whole brain	No bundle identification	25 pre-symptomatic 24 patients 49 controls	Increase of the AD and RD disperse in the brain for pre-symptomatic subjects compared to controls. This increase was found in all the brain for patients compared to controls
Phillips et al. (2016b)	WM mesh	SWM in Alzheimer	DTI-derived metrics (AD, RD)	Whole brain	No bundle identification	44 patients 47 controls	Increase of the AD and RD across most of the SWM, specially in the parahippocampal regions and the temporal and frontal lobes

(continued on next page)

Table 4 (continued)

Paper	Data type	Type of application	type of analysis	Regions	Type of bundle identification	Number of subjects	Results found
Wen et al. (2016)	Voxel	SWM in Tourette syndrome	DTI-derived metrics (FA, RD, AD and MD)	Whole brain	White matter parcellation by ROIs atlas	27 patients 27 controls	Decrease of FA and increase of RD beneath bilateral primary somatosensory cortices in Tourette syndrome children. This changes were also underneath bilateral precentral, postcentral, fronto-orbital and superior temporal auditory cortices
D'Albis et al. (2017)	Tractography	SWM in autism	DTI-derived metrics (gFA, MD, AD and RD)	Whole brain	Automatic segmentation using tractography atlas (63 bundles)	30 patients 40 controls	Increase in short distance connectivity. Decrease gFA in 6 bundles and increased in 1 bundle, increased MD in 6 bundles, increased RD in 5 bundles.
d'Albis et al. (2018)	Tractography	SWM in autism	DTI-derived metrics (gFA) and PCA	Whole brain	Automatic segmentation using tractography atlas (63 bundles)	27 patients 31 controls	Deficit in anatomical connectivity in component 3, composed of 13 bundles, left: SM-Ins, MT-SM, MT-ST, PrC-Ins, PoC-PrC_0, IP-IT, POCi-SF, IT-MT, right: SM-Ins, MOF-ST, PoC-PrC_1, PrC-SM.
Ji et al. (2018)	Tractography	SWM in schizophrenia	DTI-derived metrics (FA) and PCA	Frontal cortex	Automatic segmentation using tractography atlas (100 bundles)	31 patients 54 controls	Mean score of the second component lower in schizophrenia for 13 bundles connecting: Op, Ins; Tr, Or, orbitofrontal cortex, anterior cingulate, SF and MF.
Ji et al. (2018)	Tractography	SWM in schizophrenia and bipolar disorder	DTI-derived metrics (gFA)	Whole brain	Automatic segmentation using tractography atlas (100 bundles)	31 SZ patients 32 BD patients 54 controls	Significant gFA differences in 17 out of 65 stable SMW bundles in the frontal, parietal and temporal cortices
Phillips et al. (2018)	WM mesh	SWM damage in anti-NMDA receptor encephalitis	DTI-derived metrics (MD)	Whole brain	No bundle identification	46 patients 30 controls	MD revealed a microstructural integrity impairment in non-recovered patients versus recovered, and non recovered versus healthy controls. Increase in MD principally distributed in the frontal, temporal and parietal lobes

four bundles connecting pre and postcentral gyri from *atlas1* (PoC-PrC 0, 1, 2 and 3) using the three model/tractography configurations, compared to the original atlas bundles. We can observe that DTI reconstruction is incomplete for some bundles, while MRtrix provides the best coverage. However, depending on the analysis to be performed, DTI reconstruction could be sufficient, e. g. for the calculation of the mean FA along the bundles. Finally, the computational cost should also be considered, where DSI Studio takes less than 5 min for DTI and GQI per subject, while MRtrix takes about 48 h per subject, in the same desktop computer.

7. Applications

In the last few years, thanks to an increasing development of new tools for the study of SWM, more clinical studies regarding these structures have been made. Those studies often aim to quantify differences in pathologies like Alzheimer and dementia, autism spectrum disorders or schizophrenia.

Either by segmenting specific bundles or doing a general inspection, different studies intent to identify the relation of short connections to specific diseases. This is in general achieved by measuring diffusion values as: fractional anisotropy (FA), mean diffusivity (MD), axial diffusivity (AD) and radial diffusivity (RD), and quantifying their changes with the pathology (Alexander et al., 2007). In Table 4 a summary of clinical studies focused on SWM is presented.

Among those studies, some have revealed that the loss of integrity of the short fibers, quantified by an increased MD, contributes to a lower cognitive efficiency in healthy old adults and even more in Alzheimer patients (Gao et al., 2014). Here, the authors defined ROIs from fMRI

activations in prospective memory tasks, and then created a common ROI for the three category of subjects: healthy young (13), healthy older adults (13) and patients with mild Alzheimer disease (17). The ROI was warped into the DTI map of each subject in order to reconstruct the fibers passing through. Only short fibers measuring from 4 mm to 35 mm were selected. Increased values of the MD, RD and AD in the SWM of the temporal region have also been reported to be related to Alzheimer disease (Reginold et al., 2016). The study utilized tractography datasets calculated from the DTI data from 24 controls and 16 patients. Fibers of interest were segmented by manually placing ROIs for each lobe.

Another study showed that the values of FA are inversely related with age in the SWM for healthy individuals, especially in the fronto-parietal and occipital regions (Nazeri et al., 2015). The study was carried out using the DTI data of 141 healthy individuals, across the adult lifespan (18–86 years old), from which fibers were later reconstructed using probabilistic tractography. Only SWM fibers were selected by seeding exclusively in the cortical gray/white matter boundary and excluding DWM using exclusion masks. In order to perform the analysis, the SWM tracts were then binarized and averaged across subjects, creating a SWM probabilistic mask. The mask was used to obtain the mean FA, which was then skeletonized to perform TBSS analysis. Additionally, a MNI probabilistic atlas of cortical structures was employed to identify the SWM from frontal, parietal, occipital and temporal areas. Another study focused on age changes in SWM is presented in (Malykhin et al., 2011). The authors utilized 69 DTI datasets from subjects aged 22–84 years for studying the prefrontal white matter connections, since functions in this lobe generally decline with age. In order to do that, they manually parcellated the prefrontal white matter by placing ROIs. The results showed

that there is an increase in the AD and RD with age, starting from the 60s. Other age-focused work studied the development of the SWM in children and adolescents (Wu et al., 2014). The authors measured the FA, MD, RD and AD in 133 healthy subjects aged 10–18 years. These diffusion measures were averaged along the direction normal to the WM surface and projected into a WM template from FreeSurfer. The analysis results showed an increasing FA and decreasing MD and RD as the age increases, beneath bilateral motor sensory cortices and superior temporal auditory cortex, as well as an increase in FA and AD in bilateral orbitofrontal regions and insula.

Regarding the autism spectrum disorder (ASD), it is thought that it is generated by changes in the overall brain connectivity. Therefore, a special interest in this field has arisen not only for the study of DWM but also of the SWM. Recently a study of ASD utilized a SWM atlas of 63 bundles (Guevara et al., 2017) to identify specific bundles implicated in this pathology (d'Albis et al., 2018). These bundles were segmented from the tractography datasets of 27 patients and 31 control subjects and the mean generalized FA among them was used as a measure of integrity. It was found that a deficit of the connectivity comprising 13 bundles, mostly from frontal, temporal and parietal regions, is associated with the severity of the disorder. Similar results were found in (Sundaram et al., 2008), where the authors also found an FA significantly lower in ASD. In this study the authors only focused in the temporal lobe. The analysis was performed by manual delineation of ROIs in order to extract the fibers from whole brain tractography datasets computed from the DTI data of 50 patients and 16 controls.

Studies relating schizophrenia with changes in SWM have also been performed. A recent study used tractography datasets of 31 patients with schizophrenia and 54 healthy controls, to segment SWM bundles using the same atlas that in (d'Albis et al., Czechet et al.). This analysis exposed that there is a lower generalized FA in bundles connecting the frontal gyri, in patients with schizophrenia (Ji et al., 2018). This relationship has also been described previously by means of TBSS for the frontal and parieto-occipital connections (no specific bundles) (Nazeri et al., 2013). A different approach is the one adopted in (Phillips et al., 2011), where the authors analyzed the diffusion values by using meshes of the WM. The meshes of all subjects are aligned in terms of their sulcal lines and the FA values are obtained from the DTI image using a 10 mm sphere to average the values around each mesh vertex. The FA values were previously masked and thresholded in order to keep only those corresponding to the SWM. The method was applied to the data of 150 subjects in total, including: schizophrenia patients and their relatives, and community comparison subjects and their relatives. Results from this analysis showed a reduced SWM FA in patients specially in the left temporal and bilateral occipital regions.

The same approach described in (Phillips et al., 2011) was used in later analyses in order to study the relation of SWM in a variety of topics. In (Phillips et al., 2013) a study about the age, sex and hemispheres is performed over the data of 65 subjects. They found a decrease of FA related to age, as well as an increase of AD and RD, and also a leftward asymmetry. Another study using the same approach as a base (Phillips et al., 2011) was focused in studying the relation of SWM with Huntington's disease (Phillips et al., 2016a). The study was performed over the data of 25 pre-symptomatic subjects, 24 patients and 49 healthy controls. An increase of the AD and RD disperse in the brain was found for pre-symptomatic subjects compared to controls. For patients this increase was found in all the brain. Another work covered the relation of SWM with Alzheimer's disease (Phillips et al., 2016b). Forty-four patients and forty-seven healthy controls were analyzed. Results showed an increase of the AD and RD across most of the SWM, especially in the parahippocampal regions and the temporal and frontal lobes. Finally, in (Phillips et al., 2018) the authors studied the SWM damage in anti-NMDA receptor in encephalitis. Forty-six subjects with encephalitis and thirty controls were included in the study. The study of the MD revealed a microstructural integrity impairment in non-recovered patients versus recovered and non-recovered versus healthy controls. This increase in

MD is principally distributed in the frontal, temporal and parietal lobes.

Furthermore, some studies have been focused on the connections in the motor area, in order to investigate related disfunctionalities. Among these connections we can distinguish the bundle connecting the pre supplementary motor area and Broca's region, namely the frontal aslant tract (FAT). A study performed by Catani et al. showed that damage in this bundle has been related to progressive aphasia (Catani et al., 2013). The analysis was performed using the DTI data of 35 patients and 29 controls. Using manually drawn ROIs, the authors segmented the fiber bundles by setting them as seed regions.

Another pathology of interest in clinical studies is the bipolar disorder. In (Zhang et al., 2018c) the authors utilized DTI data from 37 bipolar patients and 42 healthy controls and probabilistic tractography to calculate population-based SWM masks. TBSS analysis was employed to measure the FA of the SWM, as well as the MD, AD and RD. The clusters found after this analysis were reported according to the atlas presented in (Guevara et al., 2017) in order to identify the cortical regions connected by them. This allowed them to find a reduced FA of the bipolar patients compared to controls, in the dorsolateral prefrontal cortex, as well as an increased MD and RD in the right frontal cortex.

The relation between SWM and psychosis has also been studied. A study focused on the fibers in the insula-temporoparietal area used DTI data from 42 patients and 45 controls to reconstruct 13 SWM bundles and analyze their differences (Hatton et al., 2014). The fiber bundles were obtained by using as seed regions ROIs from the Desikan-Killiany atlas (Desikan et al., 2006). The authors found a reduced FA in the bundle connecting the superior temporal and middle temporal gyrus, as well as an increased white matter volume in the Heschl's gyrus.

Finally, a study aimed to look for changes in the WM for children with Tourette syndrome (Wen et al., 2016). The authors combined TBSS and ROIs analyses for studying changes in FA, RD, AD and MD in DWM and SWM. A ROI atlas (Oishi et al., 2009) was used to parcellate the white matter and study the changes of DTI values locally, using the data of 27 patients and 27 controls. Regarding the SWM the results showed a decrease of FA and increase of RD beneath bilateral primary somatosensory cortices in Tourette syndrome children. These changes were also underneath bilateral precentral, postcentral, fronto-orbital and superior temporal auditory cortices.

8. Discussion and conclusion

We have presented an extensive review of the state of the art regarding the study of superficial white matter with diffusion MRI. Although the interest in their study is rather recent, an important amount of works have been published. SWM bundles are difficult to depict either from postmortem brains or tractography, however some research groups have managed to segment reliable bundles from both kind of data. Even if these studies are often limited to reduced regions of the brain, they provide a valuable source of comparison.

Different techniques and data yield different outputs. Of course none approach is perfect and depending on the level of precision in the bundle delineation, the reproducibility and variability of the bundles, the quality of the data and the study goals, one can be preferred over the others. Also, a point to consider in the decision is the study extension, in terms of the amount of regions to be analyzed. While manual positioning of ROIs offers a better delineation of the bundles extracted, it can only be applied to a reduced amount of them and most likely those with some a priori anatomical knowledge. On the other hand automatic methods allow the study of reproducible connections within the whole brain, although with a lower precision. The different types of automatic methods also have their advantages and disadvantages if we compare between them. While automatic ROI placement adds anatomical information from the cortex to the segmented fibers, these do not necessarily conform exactly to a bundle. Depending on the ROI sizes, connections between a pair of them can be composed of fibers with different shapes, sizes and positions. In contrast, clustering methods can group similar fibers, resulting in

anatomically meaningful bundles, however often no correspondence with the regions they connect is known a priori. Often these two approaches complement each other in order to obtain a better description of well-defined bundles. An example of this are the hybrid methods where the ROI extraction allows the labeling of fibers from known cortical areas, which are then clustered into anatomically meaning groups. Also this kind of method allows a restricted clustering within the regions, preventing from adding to a cluster fibers that are very similar but with a different ending. Even if no postmortem validations were performed, reproducibility analyses based on the amount of subjects in which bundles are present can be achieved.

One way or another, it is certain that most stable bundles can be segmented no matter the input data resolution of the technique employed. In an attempt to prove that, we compared three publicly available atlases, which were conceived automatically by different approaches. Even though the methods used to create the atlases differ in spatial normalization, tractography and the segmentation technique, and are based on two different databases, there is a large number of similar bundles among the three resulting atlases. We provide a compilation of 213 distinctive bundles from the three atlases, with useful information such as reproducibility and variability across subjects for three different configurations of diffusion local model and tractography methods.

Results prove that the development of more sophisticated methods is leading to a better description of SWM bundles. The current increase of available tools has allowed the inclusion of SWM in clinical studies. This grants a better and more localized understanding of the changes in the brain connectivity that trigger certain pathologies. In order to understand how the brain works we must be aware of all its components and how they relate to each other. That is the reason why it is so important to take into account the less known structures and keep developing and improving the tools for their identification and analysis. The study of SWM is still a challenge, since intersubject variability makes difficult to find patterns common to a population of subjects. As SWM is closely

related to cortical morphology, future progress will probably require a more explicit modeling of the variability of the folding patterns. Furthermore, while algorithmic progress now allow the manipulation of huge tractograms including a million streamlines, exploring further the short range connectivity may require to scale-up even further the amount of streamlines of interest.

The different clinical studies included in this review reveal that SWM is specially affected in different pathologies. These studies expose changes in different diffusion indices which are driven most likely by phenomena related to the myelination of the fibers. The SWM is specially exposed during the brain maturation as its myelination occurs mostly during the third and fourth decade of life, making the SWM more prone to lesions. Their study is very sensitive to the dMRI data quality. The advancement of dMRI equipment and methods makes it now possible to acquire datasets that allow the study of a considerable set of short fibers, ideally based on HARDI or multi-shell data. Also for a better SWM definition, more studies are required for the identification of SWM bundles using high quality databases.

Acknowledgements

This work was partially funded by the Human Brain Project, funded from the European Union's Horizon 2020 Framework Programme for Research and Innovation under the Specific Grant Agreements No. 785907 (SGA2) and No: 604102 (SGA1).

This work has also received funding by Chilean grants CONICYT FONDECYT 1190701, CONICYT PIA/Anillo de Investigación en Ciencia y Tecnología ACT172121, and the Basal Center FB0008.

HCP Data were provided by the Human Connectome Project, WU-Minn Consortium (Principal Investigators: David Van Essen and Kamil Ugurbil; 1U54MH091657) funded by the 16 NIH Institutes and Centers that support the NIH Blueprint for Neuroscience Research; and by the McDonnell Center for Systems Neuroscience at Washington University.

Appendix A

Table A.7
Desikan-Atlas ROI abbreviations

Region (gyrus)	Abb.	Region (gyrus)	Abb.
Caudal anterior cingulate	CAC	Pars orbitalis	Or
Caudal middle frontal	CMF	Pars triangularis	Tr
Cuneus	Cu	Pericalcarine	PeCa
Entorhinal	En	Postcentral	PoC
Fusiform	Fu	Posterior cingulate	PoCi
Inferior parietal	IP	Precentral	PrC
Inferior temporal	IT	Precuneus	PrCu
Isthmus cingulate	IC	Rostral anterior cingulate	RAC
Lateral occipital	LO	Rostral middle frontal	RMF
Lateral orbitofrontal	LOF	Superior frontal	SF
Lingual	Li	Superior parietal	SP
Medial orbitofrontal	MOF	Superior temporal	ST
Middle temporal	MT	Supramarginal	SM
Parahippocampal	PH	Transverse temporal	TT
Paracentral	PC	Insula	In
Pars opercularis	Op		

Abbreviations of each region in the cortical parcellation, according to the Desikan-Killiany atlas (Desikan et al., 2006). Both hemispheres contain the same regions.

Table A.8

The set of representative SWM bundles selected from the three analyzed atlases for the left hemisphere, including the bundle name, the pair of connected regions and the atlas to which the bundles belong. The reproducibility and variability of the bundles using DTI and deterministic tractography with DSI Studio (DTI), GQI and deterministic tractography with DSI Studio (GQI) and IFOD2 and probabilistic tractography using ACT + SIFT with MRtrix (MRtrix) configurations are also listed

Bundle Name	Regions	Atlas	DTI (R%)	GQI (R%)	MRtrix (R%)	DTI (RSD)	GQI (RSD)	MRtrix (RSD)
atlas_lh_MT_MT_1i	MT-MT	atlas2	100	100	100	96	102	33
atlas_lh_PrC-SM_0	PrC-SM	atlas1	100	100	100	77	108	37
atlas_lh_CMF-SF_0	CMF-SF	atlas1	100	100	100	79	97	44
atlas_lh_MT-SM_0	MT-SM	atlas1	100	100	100	86	79	49
atlas_lh_PoC-SM_0	PoC-SM	atlas1	100	100	100	85	87	31
atlas_lh_PrC-Ins_0	PrC-Ins	atlas1	100	100	100	67	73	59
atlas_lh_Op-PrC_0	Op-PrC	atlas1	100	100	100	71	82	45
atlas_lh_PoC-PrC_2	PoC-PrC	atlas1	100	100	100	76	71	41
atlas_lh_Fu_IT_Oi	Fu-IT	atlas2	100	100	100	93	61	32
atlas_lh_CMF-PrC_1	CMF-PrC	atlas1	100	100	100	72	75	39
atlas_lh_IT_IT_1i	IT-IT	atlas2	100	100	100	78	74	30
atlas_lh_Fu_Fu_Oi	Fu-Fu	atlas2	100	100	100	63	72	46
atlas_lh_PoC-SM_1	PoC-SM	atlas1	100	100	100	74	66	40
atlas_lh_SP-SM_0	SP-SM	atlas1	100	100	100	67	69	41
atlas_lh_PoCi-PrCu_1	PoCi-PrCu	atlas1	100	100	100	72	60	44
atlas_lh_RoMF_RoMF_Oi	RMF-RMF	atlas2	100	100	100	69	75	31
atlas_lh_PoC-Ins_0	PoC-Ins	atlas1	100	100	100	64	44	64
atlas_lh_IP-SP_0	IP-SP	atlas1	100	100	100	67	64	39
atlas_lh_RoMF_RoMF_1i	RMF-RMF	atlas2	100	100	100	69	68	27
atlas_lh_RMF-SF_0	RMF-SF	atlas1	100	100	100	66	70	28
atlas_lh_IP-MT_0	IP-MT	atlas1	100	100	100	59	62	41
atlas_lh_CAC-PrCu_0	CAC-PrCu	atlas1	100	100	100	65	63	29
atlas_lh_PoC-PrC_0	PoC-PrC	atlas1	100	100	100	59	59	23
atlas_lh_PoC-PrC_3	PoC-PrC	atlas1	100	100	100	46	47	44
atlas_lh_Tr_RoMF_Oi	Tr-RMF	atlas2	100	100	100	52	53	26
atlas_lh_SF_SF_0i	SF-SF	atlas2	100	100	100	44	51	29
atlas_lh_LO_LO_1i	LO-LO	atlas2	100	100	100	47	49	25
atlas_lh_RMF-SF_1	RMF-SF	atlas1	98	100	100	133	98	48
atlas_lh_IP-LO_1	IP-LO	atlas1	98	100	100	105	95	35
cluster_00346_left	CMF-RMF	atlas3	98	100	100	100	81	43
cluster_00667_left	RMF-SF	atlas3	98	100	100	83	77	33
atlas_lh_Op-SF_0	Op-SF	atlas1	98	100	100	80	49	30
atlas_lh_PoC-PrC_1	PoC-PrC	atlas1	100	98	100	79	100	44
atlas_lh_MT-ST_0	MT-ST	atlas1	100	98	100	70	78	48
cluster_00036_left	IP-SP	atlas3	100	98	100	83	71	33
atlas_lh_Op-Ins_0	Op-Ins	atlas1	100	98	100	55	64	46
atlas_lh_Tr-Ins_0	Tr-Ins	atlas1	100	98	100	66	61	30
cluster_00155_left	MT-MT	atlas3	95	100	100	150	104	34
atlas_lh_MT_MT_1i	MT-MT	atlas2	95	100	100	104	85	35
atlas_lh_MT_MT_Oi	MT-MT	atlas2	95	100	100	91	97	32
atlas_lh_SM-Ins_0	SM-Ins	atlas1	95	100	100	75	76	61
atlas_lh_CMF-PrC_0	CMF-PrC	atlas1	95	100	100	72	62	52
cluster_00460_left	PoC-PoC	atlas3	98	98	100	103	79	35
cluster_00718_left	ST-ST	atlas3	98	98	100	105	81	26
cluster_00350_left	RMF-SF	atlas3	98	98	100	90	84	27
atlas_lh_Or-Ins_0	Or-Ins	atlas1	98	98	100	73	71	30
cluster_00337_left	SM-SM	atlas3	93	100	100	119	111	38
cluster_00635_left	Op-RMF	atlas3	95	98	100	121	81	30
cluster_00427_left	SP-SP	atlas3	95	98	100	85	90	43
cluster_00556_left	IP-MT	atlas3	95	98	100	73	65	33
atlas_lh_IP-IT_0	IP-IT	atlas1	91	100	100	108	101	60
atlas_lh_ST-Ins_0	ST-Ins	atlas1	91	100	100	91	66	82
cluster_00662_left	CMF-RMF	atlas3	91	100	100	100	99	35
atlas_lh_IC-PrCu_0	IC-PrCu	atlas1	93	98	100	109	61	39
atlas_lh_IP-SP_1	IP-SP	atlas1	95	95	100	95	97	56
cluster_00554_left	IT-LO	atlas3	89	100	100	114	90	46
atlas_lh_CMF-PoC_0	CMF-PoC	atlas1	89	100	100	109	85	41
cluster_00031_left	IP-MT	atlas3	91	98	100	109	84	43
atlas_lh_CMF-Op_0	CMF-Op	atlas1	86	100	100	134	90	37
atlas_lh_PoCi-RAC_0	PoCi-RAC	atlas1	86	100	100	106	57	32
cluster_00392_left	PoC-PoC	atlas3	89	98	100	119	104	43
cluster_00385_left	CMF-RMF	atlas3	89	98	100	112	104	42
atlas_lh_PoCi-PrCu_0	PoCi-PrCu	atlas1	91	95	100	83	77	39
atlas_lh_PrC-SF_0	PrC-SF	atlas1	93	93	100	105	123	74
atlas_lh_LOF-RMF_0	LOF-RMF	atlas1	93	93	100	122	138	25
cluster_00107_left	Fu-IP	atlas3	86	98	100	126	92	50
cluster_00276_left	Op-SF	atlas3	86	98	100	105	83	36
cluster_00296_left	PoC-PrC	atlas3	86	98	100	147	109	50
atlas_lh_IT-MT_0	IT-MT	atlas1	93	90	100	112	111	52
cluster_00484_left	SM-SM	atlas3	82	100	100	142	91	38
atlas_lh_Tr-SF_0	Tr-SF	atlas1	84	98	100	116	82	41
cluster_00067_left	Cu-LO	atlas3	84	95	100	136	85	33

(continued on next column)

Table A.8 (continued)

Bundle Name	Regions	Atlas	DTI (R%)	GQI (R%)	MRtrix (R%)	DTI (RSD)	GQI (RSD)	MRtrix (RSD)
cluster_00299_left	RMF-SF	atlas3	82	95	100	125	117	54
atlas_lh_CMF-RMF_0	CMF-RMF	atlas1	86	90	100	99	110	56
atlas_lh_PoCi-SF_0	PoCi-SF	atlas1	91	85	100	115	101	56
cluster_00569_left	Fu-LO	atlas3	77	98	100	167	79	59
cluster_00414_left	PrCu-SP	atlas3	73	100	100	143	59	34
atlas_lh_MOF-ST_0	MOF-ST	atlas1	100	100	73	56	51	91
cluster_00308_left	SP-SM	atlas3	75	98	100	134	123	47
cluster_00361_left	Op-SF	atlas3	75	98	100	154	104	39
cluster_00473_left	SF-SF	atlas3	75	98	100	125	122	46
cluster_00073_left	Fu-SP	atlas3	70	98	100	209	116	58
atlas_lh_LOF-RMF_1	LOF-RMF	atlas1	82	85	100	168	107	28
atlas_lh_LOF-ST_0	LOF-ST	atlas1	93	98	75	116	79	116
cluster_00467_left	PoC-SP	atlas3	66	98	100	213	96	57
atlas_lh_LOF-Or_0	LOF-Or	atlas1	84	76	100	105	141	22
cluster_00360_left	PrC-SF	atlas3	61	98	100	185	100	56
atlas_lh_ST-TT_0	ST-TT	atlas1	61	93	100	159	91	56
cluster_00477_left	PrC-SP	atlas3	52	93	100	177	164	42
cluster_00304_left	PrC-PrC	atlas3	52	90	100	228	133	84
cluster_00015_left	IP-SM	atlas3	48	93	100	200	102	57
cluster_00294_left	PrC-SF	atlas3	59	80	100	177	134	75
cluster_00725_left	MT-ST	atlas3	41	98	100	198	66	27
cluster_00585_left	SF-SF	atlas3	41	98	100	204	109	42
cluster_00388_left	SF-SF	atlas3	45	90	100	201	106	41
cluster_00619_left	SF-SF	atlas3	34	98	100	217	133	56
cluster_00400_left	SF-SF	atlas3	55	76	100	206	105	43
cluster_00653_left	SF-SF	atlas3	36	90	100	189	103	47
cluster_00637_left	SF-SF	atlas3	32	93	100	193	124	57
atlas_lh_RAC-SF_1	RAC-SF	atlas1	43	71	100	152	124	51
atlas_lh_IP-SM_0	IP-SM	atlas1	64	44	100	196	240	58
cluster_00407_left	SF-SF	atlas3	30	78	100	227	144	46
cluster_00409_left	SF-SF	atlas3	16	90	100	293	192	47
atlas_lh_Fu-LO_0	Fu-LO	atlas1	55	51	100	156	137	72
cluster_00604_left	MOF-SF	atlas3	18	85	100	254	121	52
cluster_00478_left	PrC-SP	atlas3	18	80	100	399	128	52
cluster_00320_left	PoC-SF	atlas3	30	61	100	371	181	59
cluster_00656_left	MOF-SF	atlas3	7	80	100	451	143	60
cluster_00415_left	SF-SP	atlas3	5	73	100	626	233	45

Table A.9

The set of representative SWM bundles selected from the three analyzed atlases for the right hemisphere, including the bundle name, the pair of connected regions and the atlas to which the bundles belong. The reproducibility and variability of the bundles using DTI and deterministic tractography with DSI Studio (DTI), GQI and deterministic tractography with DSI Studio (GQI) and IFOD2 and probabilistic tractography using ACT + SIFT with MRtrix (MRtrix) configurations are also listed

Bundle Name	Regions	Atlas	DTI (R%)	GQI (R%)	MRtrix (R%)	DTI (RSD)	GQI (RSD)	MRtrix (RSD)
atlas_rh_Or-Ins_0	Or-Ins	atlas1	100	100	100	49	48	28
atlas_rh_PoC-PrC_0	PoC-PrC	atlas1	100	100	100	53	47	26
atlas_rh_PrCu-PrCu_Or	PrCu-PrCu	atlas2	100	100	100	52	61	22
atlas_rh_CAC-PrCu_0	CAC-PrCu	atlas1	100	100	100	54	51	31
atlas_rh_SF_SF_1r	SF-SF	atlas2	100	100	100	58	54	30
atlas_rh_SF_SF_2r	SF-SF	atlas2	100	100	100	63	60	23
atlas_rh_PoC-PrC_1	PoC-PrC	atlas1	100	100	100	56	63	35
atlas_rh_Op-PrC_0	Op-PrC	atlas1	100	100	100	54	63	38
atlas_rh_PoC-PrC_2	PoC-PrC	atlas1	100	100	100	50	73	46
atlas_rh_IP-IT_0	IP-IT	atlas1	100	100	100	74	71	28
atlas_rh_Fu_IT_0i	Fu-IT	atlas2	100	100	100	90	55	31
atlas_rh_SM_SM_1i	SM-SM	atlas2	100	100	100	72	76	28
atlas_rh_IP-MT_0	IP-MT	atlas1	100	100	100	70	74	32
atlas_rh_CMF-SF_1	CMF-SF	atlas1	100	100	100	67	81	37
atlas_rh_IP-SP_0	IP-SP	atlas1	100	100	100	68	75	44
atlas_rh_MT-ST_0	MT-ST	atlas1	100	100	100	79	77	34
atlas_rh_CMF-PrC_0	CMF-PrC	atlas1	100	100	100	69	84	38
atlas_rh_LOF-ST_0	LOF-ST	atlas1	100	100	100	79	47	72
atlas_rh_RMF-SF_0	RMF-SF	atlas1	100	100	100	87	94	30
atlas_rh_PrC-SM_0	PrC-SM	atlas1	100	100	100	81	96	44
atlas_rh_Op-Ins_0	Op-Ins	atlas1	98	100	100	53	56	46
atlas_rh_Tr-Ins_0	Tr-Ins	atlas1	98	100	100	82	73	32
atlas_rh_SP-SM_0	SP-SM	atlas1	98	100	100	72	81	35
atlas_rh_MT-SM_0	MT-SM	atlas1	98	100	100	67	80	44
atlas_rh_LO-SP_0	LO-SP	atlas1	98	100	100	90	75	52
atlas_rh_PoCi-PrCu_2	PoCi-PrCu	atlas1	98	100	100	111	112	41
atlas_rh_PoC-SM_0	PoC-SM	atlas1	100	98	100	73	83	40
atlas_rh_PoCi-PrCu_1	PoCi-PrCu	atlas1	100	98	100	76	89	47
atlas_rh_PrC-Ins_0	PrC-Ins	atlas1	100	98	100	97	78	63
atlas_rh_SM-Ins_0	SM-Ins	atlas1	100	98	100	87	95	72

(continued on next column)

Table A.9 (continued)

Bundle Name	Regions	Atlas	DTI (R%)	GQI (R%)	MRtrix (R%)	DTI (RSD)	GQI (RSD)	MRtrix (RSD)
cluster_00557_right	Fu-IT	atlas3	100	98	100	60	66	33
cluster_00593_right	RMF-RMF	atlas3	100	98	100	77	66	27
cluster_00319_right	CMF-SF	atlas3	100	98	100	67	75	29
cluster_00554_right	IT-LO	atlas3	100	98	100	90	77	38
atlas_rh_Op-SF_0	Op-SF	atlas1	95	100	100	82	50	33
cluster_00662_right	CMF-RMF	atlas3	95	100	100	108	88	35
atlas_rh_Tr-SF_0	Tr-SF	atlas1	95	100	100	115	94	34
cluster_00346_right	CMF-RMF	atlas3	95	100	100	119	117	39
atlas_rh_CMF-SF_0	CMF-SF	atlas1	98	98	100	79	75	41
cluster_00667_right	RMF-SF	atlas3	98	98	100	82	70	36
cluster_00350_right	RMF-SF	atlas3	98	98	100	89	85	33
cluster_00055_right	IP-SM	atlas3	98	97	100	116	87	32
atlas_rh_RMF-SF_1	RMF-SF	atlas1	93	100	100	160	93	41
cluster_00121_right	Li-PH	atlas3	95	98	100	90	63	40
cluster_00652_right	RMF-RMF	atlas3	95	98	100	122	68	39
atlas_rh_IC-PrCu_0	IC-PrCu	atlas1	98	95	100	87	97	35
atlas_rh_CMF-PrC_1	CMF-PrC	atlas1	100	93	100	80	97	54
cluster_00762_right	PrC-RMF	atlas3	91	100	100	120	103	32
cluster_00083_right	LO-SP	atlas3	91	100	100	114	98	49
cluster_00616_right	CMF-RMF	atlas3	89	100	100	109	77	38
cluster_00385_right	CMF-RMF	atlas3	89	100	100	118	118	53
cluster_00155_right	MT-MT	atlas3	91	97	100	116	91	35
atlas_rh_PoC-SP_1	PoC-SP	atlas1	95	93	100	97	105	56
atlas_rh_PoCi-RAC_0	PoCi-RAC	atlas1	86	100	100	127	49	24
cluster_00414_right	PrCu-SP	atlas3	89	98	100	128	65	30
cluster_00639_right	Op-RMF	atlas3	89	98	100	112	97	33
cluster_00071_right	Cu-Li	atlas3	89	98	100	119	107	66
atlas_rh_CAC-PoCi_0	CAC-PoCi	atlas1	84	100	100	105	80	43
cluster_00777_right	ST-ST	atlas3	84	98	100	159	73	32
atlas_rh_PrC-SP_0	PrC-SP	atlas1	89	93	100	112	100	51
atlas_rh_PoC-SP_0	PoC-SP	atlas1	89	90	100	117	119	45
atlas_rh_LOF-RMF_1	LOF-RMF	atlas1	89	90	100	154	176	37
cluster_00093_right	Cu-Li	atlas3	86	92	100	128	122	70
atlas_rh_IP-SM_0	IP-SM	atlas1	86	90	100	105	109	42
cluster_00635_right	Op-RMF	atlas3	77	98	100	150	88	33
cluster_00039_right	IP-SP	atlas3	77	98	100	155	97	36
cluster_00026_right	IP-MT	atlas3	80	95	100	131	125	49
atlas_rh_Op-Tr_0	Op-Tr	atlas1	93	80	100	119	140	43
atlas_rh_MOF-ST_0	MOF-ST	atlas1	100	100	73	64	45	83
cluster_00067_right	Cu-LO	atlas3	73	100	100	122	81	29
atlas_rh_Cu-Li_0	Cu-Li	atlas1	86	85	100	116	95	66
atlas_rh_ST-TT_0	ST-TT	atlas1	70	100	100	129	70	42
atlas_rh_PreC_SF_0i	PrC-SF	atlas2	73	98	100	159	141	47
cluster_00094_right	LO-LO	atlas3	75	95	100	176	130	40
cluster_00294_right	PrC-SF	atlas3	73	95	100	151	96	43
atlas_rh_IT-MT_1	IT-MT	atlas1	84	83	100	111	99	47
cluster_00035_right	IP-SP	atlas3	66	97	100	246	166	38
cluster_00079_right	LO-SP	atlas3	64	92	100	207	162	69
atlas_rh_Fu-LO_1	Fu-LO	atlas1	70	85	100	150	117	55
atlas_rh_IP-LO_0	IP-LO	atlas1	77	78	100	125	112	47
cluster_00101_right	Li-PeCa	atlas3	55	100	100	173	66	35
cluster_00445_right	PC-PoC	atlas3	57	98	100	213	125	35
cluster_00304_right	PrC-PrC	atlas3	57	97	100	185	124	51
atlas_rh_LOF-RMF_0	LOF-RMF	atlas1	59	95	100	165	121	31
atlas_rh_CMF-RMF_0	CMF-RMF	atlas1	70	80	100	139	120	64
cluster_00025_right	IP-SM	atlas3	50	97	100	177	92	63
cluster_00653_right	SF-SF	atlas3	57	90	100	193	126	44
cluster_00096_right	LO-Li	atlas3	52	92	100	187	84	44
cluster_00015_right	IP-ST	atlas3	48	90	100	275	137	58
atlas_rh_RAC-SF_0	RAC-SF	atlas1	52	78	100	201	116	51
cluster_00725_right	ST-ST	atlas3	25	100	100	258	91	42
cluster_00400_right	SF-SF	atlas3	50	75	100	222	148	47
cluster_00478_right	PrC-SP	atlas3	36	85	100	200	159	46
cluster_00585_right	SF-SF	atlas3	30	90	100	219	121	47
cluster_00477_right	PrC-SP	atlas3	34	85	100	225	139	37
cluster_00656_right	MOF-SF	atlas3	34	75	100	200	168	54
cluster_00407_right	SF-SF	atlas3	34	75	100	267	157	41
cluster_00619_right	SF-SF	atlas3	20	88	100	315	150	50
atlas_rh_IT-MT_2	IT-MT	atlas1	48	59	100	200	139	43
cluster_00320_right	PoC-SF	atlas3	32	64	100	300	209	51
cluster_00604_right	MOF-SF	atlas3	20	68	100	294	155	55
cluster_00415_right	SF-SP	atlas3	2	63	100	655	274	42
cluster_00479_right	PrC-SP	atlas3	0	28	100	0	306	119
atlas_rh_LOF-MOF_0	LOF-MOF	atlas1	18	7	100	294	267	60

References

- Alexander, A.L., Lee, J.E., Lazar, M., Field, A.S., 2007. Diffusion tensor imaging of the brain. *Neurotherapeutics* 4 (3), 316–329.
- Andersson, J.L., Sotiropoulos, S.N., 2015. Non-parametric representation and prediction of single-and multi-shell diffusion-weighted mri data using Gaussian processes. *Neuroimage* 122, 166–176.
- Andersson, J.L., Skare, S., Ashburner, J., 2003. How to correct susceptibility distortions in spin-echo echo-planar images: application to diffusion tensor imaging. *Neuroimage* 20 (2), 870–888.
- Andersson, J.L.R., Jenkinson, M., Smith, S., 2007. Non-linear Registration Aka Spatial Normalisation - Fmrib Technical Report Tr07ja2, Tech. Rep. FMRIB Centre, Oxford, United Kingdom.
- Basser, P.J., 1995. Inferring microstructural features and the physiological state of tissues from diffusion-weighted images. *NMR Biomed.* 8 (7), 333–344.
- Bozkurt, B., Yagmurlu, K., Middlebrooks, E.H., Karadag, A., Ovalioglu, T.C., Jagadeesan, B., Sandhu, G., Tanriover, N., Grande, A.W., 2016. Microsurgical and tractographic anatomy of the supplementary motor area complex in humans. *World Neurosurg.* 95, 99–107.
- Burks, J.D., Boettcher, L.B., Conner, A.K., Glenn, C.A., Bonney, P.A., Baker, C.M., Briggs, R.G., Pittman, N.A., O'Donoghue, D.L., Wu, D.H., et al., 2017. White matter connections of the inferior parietal lobule: a study of surgical anatomy. *Brain Behav.* 7 (4), e00640.
- Catani, M., Howard, R.J., Pajevic, S., Jones, D.K., 2002. Virtual in vivo interactive dissection of white matter fasciculi in the human brain. *Neuroimage* 17 (1), 77–94.
- Catani, M., Jones, D.K., Donato, R., Pfyfche, D.H., 2003. Occipito-temporal connections in the human brain. *Brain* 126 (9), 2093–2107.
- Catani, M., Dell'Acqua, F., Vergani, F., Malik, F., Hodge, H., Roy, P., Valabregue, R., De Schotten, M.T., 2012. Short frontal lobe connections of the human brain. *Cortex* 48 (2), 273–291.
- Catani, M., Mesulam, M.M., Jakobsen, E., Malik, F., Martersteck, A., Wieneke, C., Thompson, C.K., Thiebaut de Schotten, M., Dell'Acqua, F., Weintraub, S., et al., 2013. A novel frontal pathway underlies verbal fluency in primary progressive aphasia. *Brain* 136 (8), 2619–2628.
- Catani, M., Robertsson, N., Beyh, A., Huynh, V., de Santiago Requejo, F., Howells, H., Barrett, R.L., Aiello, M., Cavaliere, C., Dyrby, T.B., et al., 2017. Short parietal lobe connections of the human and monkey brain. *Cortex* 97, 339–357.
- Christiaens, D., Reiser, M., Dhollander, T., Sunaert, S., Suetens, P., Maes, F., 2015. Global tractography of multi-shell diffusion-weighted imaging data using a multi-tissue model. *Neuroimage* 123, 89–101.
- Chung, H.-W., Chou, M.-C., Chen, C.-Y., 2011. Principles and limitations of computational algorithms in clinical diffusion tensor mr tractography. *Am. J. Neuroradiol.* 32 (1), 3–13.
- Conturo, T.E., Lori, N.F., Cull, T.S., Akbudak, E., Snyder, A.Z., Shimony, J.S., McKinstry, R.C., Burton, H., Raichle, M.E., 1999. Tracking neuronal fiber pathways in the living human brain. *Proc. Natl. Acad. Sci. Unit. States Am.* 96 (18), 10422–10427.
- d'Albis, M.A., Guevara, P., Guevara, M., Laidi, C., Boisgontier, J., Sarrazin, S., Bouquet, C., 2018. Local structural connectivity is associated with social cognition in autism spectrum disorder. *Brain* 141 (12), 3472–3481.
- D'Albis, M.-A., Guevara, P., Guevara, M., Mangin, J.F., Poupon, C., Delphine, D., Charles, L., Houenou, J., 2017. Superficial White Matter Integrity in Autism Spectrum Disorders. *Biological Psychiatry* 81 (10), S99–S100.
- Descoteaux, M., Deriche, R., Knosche, T.R., Anwander, A., 2009. Deterministic and probabilistic tractography based on complex fibre orientation distributions. *IEEE Trans. Med. Imag.* 28 (2), 269–286.
- Desikan, R.S., Ségonne, F., Fischl, B., Quinn, B.T., Dickerson, B.C., Blacker, D., Buckner, R.L., Dale, A.M., Maguire, R.P., Hyman, B.T., et al., 2006. An automated labeling system for subdividing the human cerebral cortex on mri scans into gyral based regions of interest. *Neuroimage* 31 (3), 968–980.
- Ecker, C., Andrews, D., Dell'Acqua, F., Daly, E., Murphy, C., Catani, M., Bullmore, E.T., 2016. Relationship between cortical gyrification, white matter connectivity, and autism spectrum disorder. *Cerebral Cortex* 26 (7), 3297–3309.
- Fröhlich, F., 2016. *Network Neuroscience*. Academic Press.
- Gao, J., Cheung, R.T., Chan, Y.-S., Chu, L.-W., Mak, H.K., Lee, T.M., 2014. The relevance of short-range fibers to cognitive efficiency and brain activation in aging and dementia. *PLoS One* 9 (4), e90307.
- Glasser, M.F., Sotiropoulos, S.N., Wilson, J.A., Coalson, T.S., Fischl, B., Andersson, J.L., Xu, J., Jbabdi, S., Webster, M., Polimeni, J.R., et al., 2013. The minimal preprocessing pipelines for the human connectome project. *Neuroimage* 80, 105–124.
- Gray, H., 1878. *Anatomy of the Human Body*, vol. 8. Lea & Febiger.
- Guevara, P., Duclap, D., Marrakchi-Kacem, L., Riviere, D., Cointepas, Y., Poupon, C., Mangin, J., 2011. Accurate tractography parcellation mask using t1-weighted data rather than fa. In: *Proceedings of the International Society of Magnetic Resonance in Medicine*, p. 2018.
- Guevara, P., Duclap, D., Poupon, C., Marrakchi-Kacem, L., Fillard, P., Le Bihan, D., Leboyer, M., Houenou, J., Mangin, J.-F., 2012. Automatic fiber bundle segmentation in massive tractography datasets using a multi-subject bundle atlas. *Neuroimage* 61 (4), 1083–1099.
- Guevara, M., Román, C., Houenou, J., Duclap, D., Poupon, C., Mangin, J.F., Guevara, P., 2017. Reproducibility of superficial white matter tracts using diffusion-weighted imaging tractography. *Neuroimage* 147, 703–725.
- Hatton, S.N., Lagopoulos, J., Hermens, D.F., Hickie, I.B., Scott, E., Bennett, M.R., 2014. Short association fibres of the insula-temporoparietal junction in early psychosis: a diffusion tensor imaging study. *PLoS One* 9 (11), e112842.
- HCP. Components of the human connectome project - diffusion tractography. URL. <http://www.humanconnectome.org/study/hcp-young-adult/project-protocol/diffusion-tractography>.
- HCP Young Adult. 1200 subjects data release. URL. <https://www.humanconnectome.org/study/hcp-young-adult/document/1200-subjects-data-release>.
- Ji, E., Samuel, S., Leboyer, M., Guevara, M., Guevara, P., Poupon, C., Grigis, A., Houenou, J., 2018. T145. Alterations in superficial white matter in the frontal cortex in schizophrenia: a dwi study using a novel atlas. *Schizophr. Bull.* 44 (Suppl. 1), S172.
- Johansen-Berg, H., Behrens, T.E., 2013. *Diffusion MRI: from Quantitative Measurement to in Vivo Neuroanatomy*. Academic Press, pp. 106–117.
- Jung, J., Cloutman, L.L., Binney, R.J., Ralph, M.A.L., 2017. The structural connectivity of higher order association cortices reflects human functional brain networks. *Cortex* 97, 221–239.
- Labra, N., Guevara, P., Duclap, D., Houenou, J., Poupon, C., Mangin, J.-F., Figueroa, M., 2017. Fast automatic segmentation of white matter streamlines based on a multi-subject bundle atlas. *Neuroinformatics* 15 (1), 71–86.
- Le Bihan, D., Mangin, J.-F., Poupon, C., Clark, C.A., Pappata, S., Molko, N., Chabriat, H., 2001. Diffusion tensor imaging: concepts and applications. *J. Magn. Reson. Imag.: Off. J. Int. Soc. Magn. Reson. Med.* 13 (4), 534–546.
- Ludwig, E., Karger, J.K.S., 1957. *Atlas Cerebri Humani. The Inner Structure of the Brain Demonstrated on the Basis of Macroscopical Preparations*.
- Magro, E., Moreau, T., Seizeur, R., Gibaud, B., Morandi, X., 2012. Characterization of short white matter fiber bundles in the central area from diffusion tensor mri. *Neuroradiology* 54 (11), 1275–1285.
- Maier-Hein, K.H., Neher, P.F., Houde, J.-C., Côté, M.-A., Garyfallidis, E., Zhong, J., Chamberland, M., Yeh, F.-C., Lin, Y.-C., Ji, Q., et al., 2017. The challenge of mapping the human connectome based on diffusion tractography. *Nat. Commun.* 8 (1), 1349.
- Malykhin, N., Vahidy, S., Michielse, S., Coupland, N., Camicioli, R., Seres, P., Carter, R., 2011. Structural organization of the prefrontal white matter pathways in the adult and aging brain measured by diffusion tensor imaging. *Brain Struct. Funct.* 216 (4), 417.
- Mangin, J.-F., Lebenberg, J., Lefranc, S., Labra, N., Auzias, G., Labit, M., Guevara, M., Mohlberg, H., Roca, P., Guevara, P., et al., 2016. *Spatial Normalization of Brain Images and beyond*.
- Meynert, T., 1885. *Psychiatry: A Clinical Treatise on Diseases of the Fore-Brain: the Anatomy, Physiology, and Chemistry of the Brain*.
- Mori, S., Van Zijl, P.C., 2002. Fiber tracking: principles and strategies—a technical review. *NMR Biomed.: Int. J. Devoted Dev. Appl. Magn. Reson. In Vivo* 15 (7–8), 468–480.
- Nazeri, A., Chakravarty, M.M., Felsky, D., Lobaugh, N.J., Rajji, T.K., Mulsant, B.H., Voineskos, A.N., 2013. Alterations of superficial white matter in schizophrenia and relationship to cognitive performance. *Neuropsychopharmacology* 38 (10), 1954.
- Nazeri, A., Chakravarty, M.M., Rajji, T.K., Felsky, D., Rotenberg, D.J., Mason, M., Xu, L.N., Lobaugh, N.J., Mulsant, B.H., Voineskos, A.N., 2015. Superficial white matter as a novel substrate of age-related cognitive decline. *Neurobiol. Aging* 36 (6), 2094–2106.
- Oishi, K., Zilles, K., Amunts, K., Faria, A., Jiang, H., Li, X., Akhter, K., Hua, K., Woods, R., Toga, A.W., et al., 2008. Human brain white matter atlas: identification and assignment of common anatomical structures in superficial white matter. *Neuroimage* 43 (3), 447–457.
- Oishi, K., Faria, A., Jiang, H., Li, X., Akhter, K., Zhang, J., Hsu, J.T., Miller, M.L., van Zijl, P.C., Albert, M., et al., 2009. Atlas-based whole brain white matter analysis using large deformation diffeomorphic metric mapping: application to normal elderly and alzheimer's disease participants. *Neuroimage* 46 (2), 486–499.
- Ouyang, M., Jeon, T., Mishra, V., Du, H., Wang, Y., Peng, Y., Huang, H., 2016. Global and regional cortical connectivity maturation index (ccmi) of developmental human brain with quantification of short-range association tracts. In: *Medical Imaging 2016: Biomedical Applications in Molecular, Structural, and Functional Imaging*, vol. 9788. International Society for Optics and Photonics, p. 97881B.
- Ouyang, M., Kang, H., Detre, J.A., Roberts, T.P., Huang, H., 2017. Short-range connections in the developmental connectome during typical and atypical brain maturation. *Neurosci. Biobehav. Rev.* 83, 109–122.
- O'Donnell, L.J., Kubicki, M., Shenton, M.E., Dreusicke, M.H., Grimson, W.E.L., Westin, C.-F., 2006. A method for clustering white matter fiber tracts. *Am. J. Neuroradiol.* 27 (5), 1032–1036.
- O'Donnell, L.J., Wells, W.M., Golby, A.J., Westin, C.-F., 2012. Unbiased groupwise registration of white matter tractography. In: *International Conference on Medical Image Computing and Computer-Assisted Intervention*. Springer, pp. 123–130.
- O'Donnell, L.J., Golby, A.J., Westin, C.-F., 2013. Fiber clustering versus the parcellation-based connectome. *Neuroimage* 80, 283–289.
- Phillips, O.R., Nuechterlein, K.H., Asarnow, R.F., Clark, K.A., Cabeen, R., Yang, Y., Woods, R.P., Toga, A.W., Narr, K.L., 2011. Mapping corticocortical structural integrity in schizophrenia and effects of genetic liability. *Biol. Psychiatr.* 70 (7), 680–689.
- Phillips, O.R., Clark, K.A., Luders, E., Azhri, R., Joshi, S.H., Woods, R.P., Mazziotta, J.C., Toga, A.W., Narr, K.L., 2013. Superficial white matter: effects of age, sex, and hemisphere. *Brain Connect.* 3 (2), 146–159.
- Phillips, O.R., Joshi, S.H., Squitieri, F., Sanchez-Castaneda, C., Narr, K., Shattuck, D.W., Caltagirone, C., Sabatini, U., Di Paola, M., 2016a. Major superficial white matter abnormalities in huntington's disease. *Front. Neurosci.* 10, 197.
- Phillips, O.R., Joshi, S.H., Piras, F., Orfei, M.D., Iorio, M., Narr, K.L., Shattuck, D.W., Caltagirone, C., Spalletta, G., Di Paola, M., 2016b. The superficial white matter in alzheimer's disease. *Hum. Brain Mapp.* 37 (4), 1321–1334.
- Phillips, O.R., Joshi, S.H., Narr, K.L., Shattuck, D.W., Singh, M., Di Paola, M., Ploner, C.J., Prüss, H., Paul, F., Finke, C., 2018. Superficial white matter damage in anti-nmda receptor encephalitis. *J. Neurol. Neurosurg. Psychiatr.* 89 (5), 518–525.
- Pierpaoli, C., Jezzard, P., Basser, P.J., Barnett, A., Di Chiro, G., 1996. Diffusion tensor mr imaging of the human brain. *Radiology* 201 (3), 637–648.

- Pron, A., Brun, L., Deruelle, C., Coulon, O., 2018. Dense and structured representations of u-shape fiber connectivity in the central sulcus. In: Biomedical Imaging (ISBI 2018), 2018 IEEE 15th International Symposium on. IEEE, pp. 700–703.
- Reginold, W., Luedke, A.C., Itorralba, J., Fernandez-Ruiz, J., Islam, O., Garcia, A., 2016. Altered superficial white matter on tractography mri in alzheimer's disease. *Dement. Geriatr. Cognit. Disord. Extra* 6 (2), 233–241.
- Rojkova, K., Volle, E., Urbanski, M., Humbert, F., Dell'Acqua, F., De Schotten, M.T., 2016. Atlasing the frontal lobe connections and their variability due to age and education: a spherical deconvolution tractography study. *Brain Struct. Funct.* 221 (3), 1751–1766.
- Román, C., Guevara, M., Valenzuela, R., Figueroa, M., Houenou, J., Duclap, D., Poupon, C., Mangin, J.-F., Guevara, P., 2017. Clustering of whole-brain white matter short association bundles using hardi data. *Front. Neuroinf.* 11, 73.
- Román, C., Cárdenas, N., Poupon, C., Mangin, J.F., Guevara, P., 2019. The effect of the number of fibers in tractography reconstruction of white matter bundles. In: 2019 41st Annual International Conference of the IEEE Engineering in Medicine and Biology Society (EMBC), pp. 2825–2829.
- Schmitt, B., Lebois, A., Duclap, D., Guevara, P., Poupon, F., Rivière, D., Cointepas, Y., LeBihan, D., Mangin, J.-F., Poupon, C., 2012. Connect/archi: an open database to infer atlases of the human brain connectivity. In: ESMRMB 2012.
- Shukla, D.K., Keehn, B., Smylie, D.M., Müller, R.A., 2011. Microstructural abnormalities of short-distance white matter tracts in autism spectrum disorder. *Neuropsychologia* 49 (5), 1378–1382.
- Smith, R., Tournier, J.-D., Calamante, F., Connelly, A., 2012. Anatomically-constrained tractography: improved diffusion mri streamlines tractography through effective use of anatomical information. *Neuroimage* 62 (3), 1924–1938.
- Smith, R.E., Tournier, J.-D., Calamante, F., Connelly, A., 2013. Sift: spherical-deconvolution informed filtering of tractograms. *Neuroimage* 67, 298–312.
- Sporns, O., Tononi, G., Kötter, R., 2005. The human connectome: a structural description of the human brain. *PLoS Comput. Biol.* 1 (4), e42.
- Sundaram, S.K., Kumar, A., Makki, M.I., Behen, M.E., Chugani, H.T., Chugani, D.C., 2008. Diffusion tensor imaging of frontal lobe in autism spectrum disorder. *Cerebr. Cortex* 18 (11), 2659–2665.
- Tournier, J.-D., Calamante, F., Connelly, A., 2007. Robust determination of the fibre orientation distribution in diffusion mri: non-negativity constrained super-resolved spherical deconvolution. *Neuroimage* 35 (4), 1459–1472.
- Vergani, F., Lacerda, L., Martino, J., Attems, J., Morris, C., Mitchell, P., de Schotten, M.T., Dell'Acqua, F., 2014a. White matter connections of the supplementary motor area in humans. *J. Neurol. Neurosurg. Psychiatry* 85 (12), 1377–1385.
- Vergani, F., Mahmood, S., Morris, C.M., Mitchell, P., Forkel, S.J., 2014b. Intralobar fibres of the occipital lobe: a post mortem dissection study. *Cortex* 56, 145–156.
- Wakana, S., Jiang, H., Nagae-Poetscher, L.M., Van Zijl, P.C., Mori, S., 2004. Fiber tract-based atlas of human white matter anatomy. *Radiology* 230 (1), 77–87.
- Wassermann, D., Bloy, L., Kanterakis, E., Verma, R., Deriche, R., 2010. Unsupervised white matter fiber clustering and tract probability map generation: applications of a Gaussian process framework for white matter fibers. *Neuroimage* 51 (1), 228–241.
- Wen, H., Liu, Y., Wang, J., Reikik, I., Zhang, J., Zhang, Y., Tian, H., Peng, Y., He, H., 2016. Combining tract-and atlas-based analysis reveals microstructural abnormalities in early tourette syndrome children. *Hum. Brain Mapp.* 37 (5), 1903–1919.
- Wu, M., Lu, L.H., Lowes, A., Yang, S., Passarotti, A.M., Zhou, X.J., Pavuluri, M.N., 2014. Development of superficial white matter and its structural interplay with cortical gray matter in children and adolescents. *Hum. Brain Mapp.* 35 (6), 2806–2816.
- Wu, Y., Sun, D., Wang, Y., Wang, Y., Wang, Y., 2016. Tracing short connections of the temporo-parieto-occipital region in the human brain using diffusion spectrum imaging and fiber dissection. *Brain Res.* 1646, 152–159.
- Yeh, F.-C., Tseng, W.-Y.I., 2011. Ntu-90: a high angular resolution brain atlas constructed by q-space diffeomorphic reconstruction. *Neuroimage* 58 (1), 91–99.
- Yeh, F.-C., Wedeen, V.J., Tseng, W.-Y.I., 2010. Generalized q-sampling imaging. *IEEE Trans. Med. Imag.* 29 (9), 1626–1635.
- Yeh, F.-C., Verstynen, T.D., Wang, Y., Fernández-Miranda, J.C., Tseng, W.-Y.I., 2013. Deterministic diffusion fiber tracking improved by quantitative anisotropy. *PLoS One* 8 (11), e80713.
- Yeh, F.-C., Panesar, S., Fernandes, D., Meola, A., Yoshino, M., Fernandez-Miranda, J.C., Vettel, J.M., Verstynen, T., 2018. Population-averaged atlas of the macroscale human structural connectome and its network topology. *Neuroimage* 178, 57–68.
- Zhang, S., Correia, S., Laidlaw, D.H., 2008. Identifying white-matter fiber bundles in dti data using an automated proximity-based fiber-clustering method. *IEEE Trans. Visual. Comput. Graph.* 14 (5), 1044–1053.
- Zhang, Y., Zhang, J., Oishi, K., Faria, A.V., Jiang, H., Li, X., Akhter, K., Rosa-Neto, P., Pike, G.B., Evans, A., et al., 2010. Atlas-guided tract reconstruction for automated and comprehensive examination of the white matter anatomy. *Neuroimage* 52 (4), 1289–1301.
- Zhang, T., Chen, H., Guo, L., Li, K., Li, L., Zhang, S., Shen, D., Hu, X., Liu, T., 2014. Characterization of u-shape streamline fibers: methods and applications. *Med. Image Anal.* 18 (5), 795–807.
- Zhang, F., Wu, Y., Norton, I., Rigolo, L., Rathi, Y., Makris, N., O'Donnell, L.J., 2018a. An anatomically curated fiber clustering white matter atlas for consistent white matter tract parcellation across the lifespan. *Neuroimage* 179, 429–447.
- Zhang, F., Savadjiev, P., Cai, W., Song, Y., Rathi, Y., Tunç, B., Parker, D., Kapur, T., Schultz, R.T., Makris, N., et al., 2018b. Whole brain white matter connectivity analysis using machine learning: an application to autism. *Neuroimage* 172, 826–837.
- Zhang, S., Wang, Y., Deng, F., Zhong, S., Chen, L., Luo, X., Qiu, S., Chen, P., Chen, G., Hu, H., et al., 2018c. Disruption of superficial white matter in the emotion regulation network in bipolar disorder. *NeuroImage: Clin.* 20, 875–882.
- Zhang, F., Wu, Y., Norton, I., Rathi, Y., Golby, A.J., O'Donnell, L.J., 2019. Test-retest reproducibility of white matter parcellation using diffusion mri tractography fiber clustering. *Hum. Brain Mapp.* 40 (10), 3041–3057.
- Zikopoulos, B., Barbas, H., 2013. Altered neural connectivity in excitatory and inhibitory cortical circuits in autism. *Front. Hum. Neurosci.* 7, 609.